

Article

Addition of Small Electrophiles to NHC-stabilized Disilicon(0): A Revisit of the Isolobal Concept in Low-Valent Silicon Chemistry

Marius I. Arz, Martin Straßmann, Daniel Geiß, Gregor Schnakenburg, and Alexander C. Filippou

J. Am. Chem. Soc., **Just Accepted Manuscript** • DOI: 10.1021/jacs.6b01018 • Publication Date (Web): 15 Mar 2016

Downloaded from <http://pubs.acs.org> on March 16, 2016

Just Accepted

“Just Accepted” manuscripts have been peer-reviewed and accepted for publication. They are posted online prior to technical editing, formatting for publication and author proofing. The American Chemical Society provides “Just Accepted” as a free service to the research community to expedite the dissemination of scientific material as soon as possible after acceptance. “Just Accepted” manuscripts appear in full in PDF format accompanied by an HTML abstract. “Just Accepted” manuscripts have been fully peer reviewed, but should not be considered the official version of record. They are accessible to all readers and citable by the Digital Object Identifier (DOI®). “Just Accepted” is an optional service offered to authors. Therefore, the “Just Accepted” Web site may not include all articles that will be published in the journal. After a manuscript is technically edited and formatted, it will be removed from the “Just Accepted” Web site and published as an ASAP article. Note that technical editing may introduce minor changes to the manuscript text and/or graphics which could affect content, and all legal disclaimers and ethical guidelines that apply to the journal pertain. ACS cannot be held responsible for errors or consequences arising from the use of information contained in these “Just Accepted” manuscripts.



ACS Publications

Addition of Small Electrophiles to NHC-stabilized Disilicon(0): A Revisit of the Isolobal Concept in Low-Valent Silicon Chemistry

Marius I. Arz, Martin Straßmann, Daniel Geiß, Gregor Schnakenburg, and Alexander C. Filippou*

Institute of Inorganic Chemistry, University of Bonn, Gerhard-Domagk-Straße 1, D-53121 Bonn, Germany

Abstract: Protonation and alkylation of (Idipp)Si=Si(Idipp) (**1**) afforded the mixed-valent disilicon(I)-borates [(Idipp)(R)Si^{II}=Si⁰(Idipp)][B(Ar^F)₄] (**1R**[B(Ar^F)₄]; R = H, Me, Et; Ar^F = C₆H₃-3,5-(CF₃)₂; Idipp = C[N(C₆H₃-2,6-*i*Pr₂)CH]₂) as red to orange colored, highly air-sensitive solids, which were characterized by single-crystal X-ray diffraction, IR spectroscopy and multinuclear NMR spectroscopy. Dynamic NMR studies in solution revealed a degenerate isomerisation (topomerisation) of the “σ-bonded” tautomers of **1H**[B(Ar^F)₄], which proceeds according to quantum chemical calculations via a NHC-stabilized (NHC = N-heterocyclic carbene) disilahydronium ion (“π-bonded” isomer) and is reminiscent of the degenerate rearrangement of carbenium ions formed upon protonation of olefins. The topomerisation of **1H**[B(Ar^F)₄] provides the first example of a reversible 1,2-H migration along a Si=Si bond observed in a molecular system. In contrast, **1Me**[B(Ar^F)₄] adopts a “rigid” structure in solution due to the higher energy required for the interconversion of the “σ-bonded” isomer into a putative NHC-stabilized disilamethonium ion. Addition of alkali metal borates to **1** afforded the alkali metal disilicon(0) borates **1M**[BAr₄] (M = Li, Ar = C₆F₅; M = Na, Ar = Ar^F) as brown, air-sensitive solids. Single-crystal X-ray diffraction analyses and NMR spectroscopic studies of **1M**[BAr₄] suggest in concert with quantum chemical calculations that encapsulation of the alkali metal cations in the cavity of **1** predominantly occurs via electrostatic cation π-interactions with the Si=Si π-bond and the peripheral NHC aryl rings. Displacement of the [Si(NHC)] fragments by the isolobal fragments [PR] and [SiR][−] interrelates the cations [(NHC)(R)Si=Si(NHC)]⁺ to a series of familiar, multiply bonded Si and P compounds as verified by analyses of their electronic structures.

1. Introduction

Stabilization of highly reactive low-valent main-group element species by utilizing N-heterocyclic carbenes (NHCs) as particularly strong σ -donors led in recent years to a plethora of novel compounds with intriguing synthetic potential and to a flourishing, rapidly developing field in chemistry.¹ Appealing examples in low-valent silicon chemistry include the Si^0 compounds $(\text{Idipp})\text{Si}=\text{Si}(\text{Idipp})$ (**1**, $\text{Idipp} = \text{C}[\text{N}(\text{dipp})\text{CH}]_2$, $\text{dipp} = \text{C}_6\text{H}_3\text{-2,6-}i\text{Pr}_2$)² and $\text{Si}(\text{bNHC})$ ($\text{bNHC} = \text{bidentate N-heterocyclic carbene}$),³ the Si^{I} halides $\text{Si}_2\text{X}_2(\text{Idipp})_2$ ($\text{X} = \text{Cl},^2 \text{Br},^4 \text{I}^4$), the NHC-adducts of the Si^{II} halides SiX_2 ($\text{X} = \text{Cl} - \text{I}$),⁵ $\text{Si}(\text{X})\text{R}$ ($\text{X} = \text{Cl}, \text{H}$; $\text{R} = \text{aryl}, \text{amino}$),⁶ and of the disilenyldisilylene $\text{SiR}(\text{SiR}=\text{SiR}_2)$,⁷ or the NHC-stabilized cations $[\text{Si}_2]^+$,⁸ $[\text{SiR}]^+$ and Si^{2+} .^{5d,6e,9} The same strategy also enabled to trap silagermenyldienes ($\text{R}_2\text{Si}=\text{Ge}$),¹⁰ phosphasilynyldienes ($\text{RP}=\text{Si}$)¹¹ and disilavinylidenes ($\text{R}_2\text{Si}=\text{Si}$).¹²

Analysis of the bonding between main-group elements and NHCs raised a controversial debate in the literature.¹³ G. Frenking et al. viewed **1** as a Si_2 molecule that is trapped in its excited ($^1\Delta_g$) electronic state by two NHCs, and calculated the donor-acceptor $\text{Si}-\text{C}_{\text{NHC}}$ interactions in **1** using the EDA-NOCV method.¹⁴ Although this donor-acceptor model provides a simplified interpretation of the bonding in **1**, which has been also used to rationalize the bonding in other NHC-stabilized diatomic molecules,^{14,15} it is not adequate to forecast the reactivity of **1** given the considerably higher energy of the ($^1\Delta_g$) electronic state of Si_2 than that of its triplet ground-state configuration ($\text{X}^3\Sigma_g^-$)¹⁶ and the rather large $\text{Si}-\text{C}_{\text{NHC}}$ bond dissociation energies,¹⁷ which prevented so far to use **1** as a source of Si_2 in reactions.

An alternative view of **1** was recently presented in an experimental and theoretical study by our group, which uncovered the similarity of the electronic structure of **1** with that of the diphosphene (*E*)- $\text{Mes}^*\text{P}=\text{PMes}^*$ ($\text{Mes}^* = \text{C}_6\text{H}_2\text{-2,4,6-}i\text{Bu}_3$) and the NHC-stabilized phosphasilynylidene $(\text{Idipp})\text{Si}=\text{PMes}^*$, with all three compounds showing a similar sequence of the frontier orbitals with almost isoenergetic $n_x(\text{E}-\text{E})$ lone pair ($\text{E} = \text{Si}$ or P)¹⁸ and $\pi(\text{E}=\text{E})$ orbitals as the HOMO and the HOMO-1, respectively.¹¹ This relationship, which can be traced back to the isolobal analogy¹⁹ of the fragments $[\text{Si}(\text{NHC})]$, $[\text{PR}]$ and $[\text{SiR}]^-$, allowed also to rationalize the experimentally determined structure of the 1e-oxidation product of **1** ($[(\text{Si}_2(\text{Idipp})_2)]^+$), and to interrelate its electronic structure with that of the disilyne radical anions $[\text{Si}_2\text{R}_2]^-$.^{8,20}

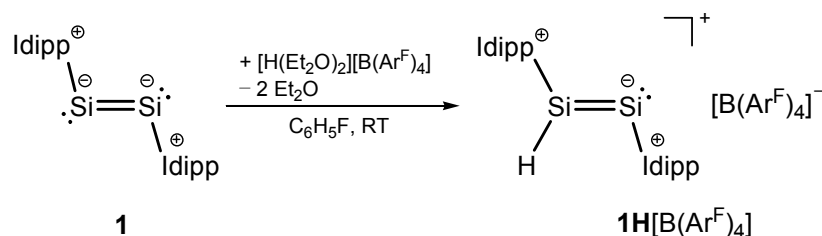
Additional support for this view can be found by comparing the reactivity of the isolobal compounds. Remarkably, diphosphenes have been shown to adopt either η^1 , η^2 or $\mu(\eta^1;\eta^1)$ coordination modes in complexes with coinage-metals,²¹ and similar coinage metal complexes of the disilicon(0) compound **1** of the general formulas $[\text{MCl}(\eta^1\text{-1})]$, $[\text{M}(\eta^2\text{-1})][\text{B}(\text{C}_6\text{F}_5)_4]$ and $[\text{M}_2\text{Cl}_2-\mu-(1\kappa\text{Si}^1:2\kappa\text{Si}^2\text{-1})]$ ($\text{M} = \text{coinage metal atom}$) have been reported recently by G. Robinson et al. and our group.²²

In comparison, reactivity studies of diphosphenes towards simple electrophiles such as H^+ or R^+ are very limited. Methylation of $(E)\text{-Mes}^*\text{P}=\text{PMes}^*$ has been reported to give the isolable phosphanylphosphenium cation $[\text{Mes}^*(\text{Me})\text{P}=\text{PMes}^*]^+$,^{23a} whereas attempts to detect the corresponding protonation product $[\text{Mes}^*(\text{H})\text{P}=\text{PMes}^*]^+$ failed.^{21b,23b}

This prompted us to study the hitherto unexplored reactivity of **1** towards the electrophiles H^+ and R^+ and alkali metal cations. Herein, we report on the protonation and electrophilic alkylation of **1** leading to the disilicon(I) compounds $[(\text{Idipp})(\text{R})\text{Si}=\text{Si}(\text{Idipp})]\text{A}$ ($\text{R} = \text{H}, \text{Me}, \text{Et}$; $\text{A} = \text{borate anion}$) as well as the reactions of **1** with alkali metal borates, yielding the alkali metal disilicon(0) borates $[\text{Si}_2(\text{M})(\text{Idipp})_2]\text{A}$ ($\text{M} = \text{Li}, \text{Na}$). All products were thoroughly studied by a combination of experimental and theoretical methods. In addition, we report on a detailed quantum chemical study, which corroborates the isolobal analogy of the cations $[(\text{Idipp})(\text{R})\text{Si}=\text{Si}(\text{Idipp})]^+$ to a series of familiar, multiply bonded Si and P compounds.

2. Results and discussion

2.1 Protonation of $(\text{Idipp})\text{Si}=\text{Si}(\text{Idipp})$. The hydridodisilicon(I)-borate $[(\text{Idipp})(\text{H})\text{Si}=\text{Si}(\text{Idipp})][\text{B}(\text{Ar}^F)_4]$ (**1H** $[\text{B}(\text{Ar}^F)_4]$) was obtained selectively upon protonation of **1** with Brookhart's acid $[\text{H}(\text{Et}_2\text{O})_2][\text{B}(\text{Ar}^F)_4]$, $\text{Ar}^F = \text{C}_6\text{H}_3\text{-3,5-(CF}_3)_2$)²⁴ in fluorobenzene and isolated after crystallization from a fluorobenzene / *n*-hexane mixture at -30°C as a dark red, highly air-sensitive solid in 80 % yield (Scheme 1) (see supporting information (SI), chapter 2.1). Compound **1H** $[\text{B}(\text{Ar}^F)_4]$ is a thermally robust solid, which decomposes upon melting in a vacuum-sealed glass capillary at 221°C . Slow decomposition of **1H** $[\text{B}(\text{Ar}^F)_4]$ to $[\text{IdippH}][\text{B}(\text{Ar}^F)_4]$ and other unidentified products was however observed by ^1H NMR spectroscopy in $\text{THF-}d_8$ solution at room temperature within 24 h.



Scheme 1. Synthesis of compound **1H** $[\text{B}(\text{Ar}^F)_4]$. Formal charges are encircled.

The solid-state structure of **1H** $[\text{B}(\text{Ar}^F)_4]$ was determined by single-crystal X-ray diffraction, and confirmed that the cations **1H** $^+$ (Figure 1) are well separated from the borate anions. The closest $\text{Si}\cdots\text{F}$ contacts of $4.99(1)\text{ \AA}$ are significantly longer than the sum of the van der Waals radii of silicon and fluorine (3.6 \AA).²⁵ The H85 atom was localized in the difference Fourier map and isotropically refined. It is σ -bonded to the Si1 atom, which is trigonal planar bonded

according to the sum of bond angles of $360(1)^\circ$. The torsion angles $C1-Si1-Si2-C28$ and $H85-Si1-Si2-C28$ of $177.61(8)^\circ$ and $-6(1)^\circ$ indicate a planar $C_{NHC}-Si(H)-Si-C_{NHC}$ core with a *trans*-arrangement of the NHC-substituents. The Si1-bonded central ring of the NHC-substituent adopts a coplanar conformation ($\varphi_{NHC1} = 8.60(6)^\circ$) with respect to the $C_{NHC}-Si-Si-C_{NHC}$ plane, whereas the Si2-bonded NHC-substituent is perpendicularly oriented ($\varphi_{NHC2} = 71.06(6)^\circ$) (Figure 1, right).²⁶

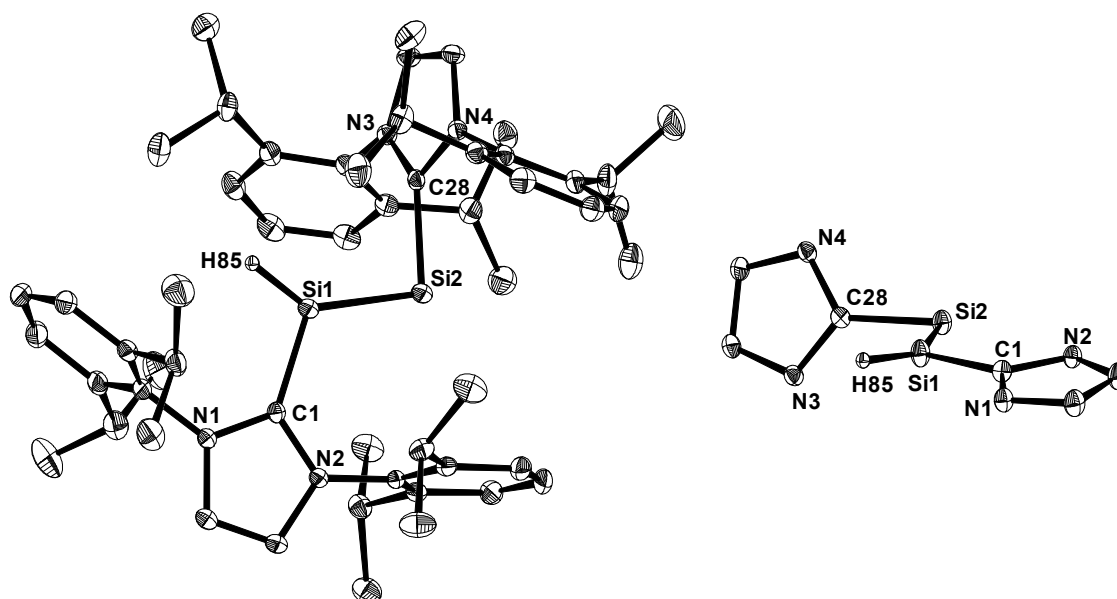


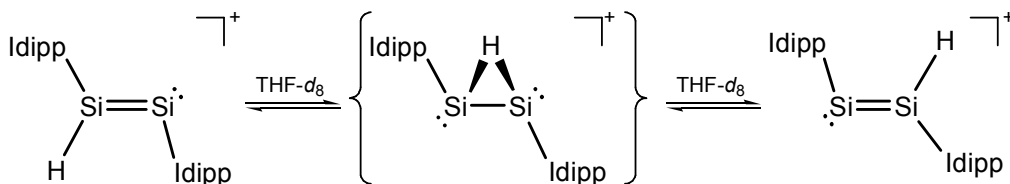
Figure 1. Left: DIAMOND plot of the molecular structure of the cation $1H^+$ in the crystal lattice of $1H[B(Ar^F)_4]$ at 123(2) K. Thermal ellipsoids are set at 30 % probability. Hydrogen atoms, except the Si1-bonded H85 atom, were omitted for clarity. Selected bond lengths [Å], bond angles [$^\circ$] and torsion angles [$^\circ$]: Si1–C1 1.882(2), Si1–Si2 2.1873(8), Si2–C28 1.940(2), Si1–H85 1.32(2); C1–Si1–Si2 116.73(7), C1–Si1–H1 106(1), Si2–Si1–H85 138(1), C28–Si2–Si1 95.34(6); C1–Si1–Si2–C28 177.61(8), H85–Si1–Si2–C28 $-6(1)$. Right: Different view of $1H^+$ illustrating the different orientation of the Si-bonded NHC-rings; hydrogen atoms (except the H85 atom) and the N-bonded dipp substituents were omitted for clarity.

The Si=Si bond (2.1873(8) Å) of $1H^+$ compares well with those of the isolobal compounds (Z)-Tbb(Br)Si=Si(Sldipp) (2.167(2) Å, Tbb = $C_6H_2-2,6-[CH(SiMe_3)_2]_2-4-tBu$, Sldipp = $C[N(dipp)CH_2]_2$),¹² $(IMe_4)(R^{Si})Si=SiR^{Si}$ (2.1989(6) Å, $IMe_4 = C[N(Me)CMe]_2$, $R^{Si} = Si/Pr[CH(SiMe_3)_2]_2$),²⁷ $[Li(dme)_3][R^{Si}(H)Si=SiR^{Si}]$ (2.2034(9) Å, dme = 1,2-dimethoxyethane)²⁸ and $[(Idipp)(I)Si=Si(Idipp)][B(C_6F_5)_4]$ (2.1739(9) Å),⁴ but is shorter (1.9 %) than that of **1** (2.229(1) Å)² and $Si_2(Sldipp)_2$ (2.2323(8) Å).²⁹ Shortening of the Si=Si bond of **1** upon protonation can be rationalized according to comparative natural bonding orbital (NBO) analyses of 1_{calc} and $1H^+_{calc}$ (see SI, Tables S7 and S8) with the increased s-character of the hybrid orbital on the Si1 atom employed in the Si–Si σ -bond. Consistently, $1H^+$ displays a shortened Si1–C1 bond (1.882(2) Å) and a widened C1–Si1–Si2 angle ($116.73(7)^\circ$) compared

to **1** (Si–C_{NHC}: 1.927(2) Å; ∠C_{NHC}–Si–Si# = 93.37(5)°).² Another salient feature of the structure of **1H**⁺ is the narrow C28–Si2–Si1 angle of 95.34(6)°, which suggests the presence of a lone pair of high s-character at the Si2 atom, in full agreement with the results of the NBO analysis of **1H**⁺_{calc} (see SI, Table S8).

The ATR FTIR spectrum of a solid state sample of **1H**[B(Ar^F)₄] displays a weak absorption band at 2142 cm^{−1}, which is assigned to the ν(Si–H) stretching vibration (see SI, Figure S1). This band does not appear in the IR spectrum of the deuterated derivative [(Idipp)(D)Si=Si(Idipp)][B(Ar^F)₄] (**1D**[B(Ar^F)₄]), which was analogously obtained from **1** and [D(Et₂O)₂][B(Ar^F)₄] (see SI, chapter 2.2). However, the ν(Si–D) absorption band of **1D**[B(Ar^F)₄], which is expected to appear at 1541 cm^{−1}, was not detected due to its weak intensity and superimposition with other absorption bands in this region. The ν(Si–H) absorption band of **1H**[B(Ar^F)₄] emerges at a similar wavenumber as the ν(Si–H) absorptions of the 1,2-dihydridodisilenes (*E*)-Si₂H₂R₂ (ν(Si–H) = 2160 cm^{−1}, R = Bbp = C₆H₃-2,6-[CH(SiMe₃)₂]₂; ν(Si–H) = 2151 cm^{−1}, R = Bbt = C₆H₂-2,6-[CH(SiMe₃)₂]₂-4-C(SiMe₃)₃, both in KBr),³⁰ but appears at lower wavenumbers than those of hydridosilanes (e.g. RSiH_nCl_{3−n} (n = 1 – 3): ν(Si–H) = 2171 – 2240 cm^{−1}; R = C₆H₃-2,6-(C₆H₂-2,4,6-*i*Pr₃)₂).³¹

Notably, **1H**[B(Ar^F)₄] is fluxional on the NMR timescale. The dynamic process was studied by variable temperature ¹H, ¹³C{¹H} and ²⁹Si NMR spectroscopy in THF-*d*₈ and involves a degenerate isomerization (topomerization)³² between the “σ-bonded” tautomers of **1H**⁺, which leads to an exchange of the two heterotopic silicon sites in solution (Scheme 2). Thus, two well separated ²⁹Si doublet signals at δ = 69.4 ppm and 125.4 ppm are observed in the slow exchange limit ²⁹Si NMR spectrum of **1H**[B(Ar^F)₄] in THF-*d*₈ at 213 K for the three-coordinated (Si1) and two-coordinated (Si2) silicon atom, respectively (Figure 2, left). In comparison, no ²⁹Si NMR signal was detected in the ²⁹Si NMR spectrum of **1H**[B(Ar^F)₄] in THF-*d*₈ at 333 K, even after long accumulation time, due to rapid site exchange.



Scheme 2. Topomerization of **1H**[B(Ar^F)₄] in THF-*d*₈ solution. The tentative intermediate, a NHC-stabilized disilahydronium ion, is depicted in curly brackets. The [B(Ar^F)₄][−] counteranion and formal charges were omitted for simplicity.

Both ²⁹Si NMR signals of **1H**[B(Ar^F)₄] appear in the slow exchange limit spectrum at similar frequencies as those of the structurally related cations **1Me**⁺ and **1Et**⁺ (see Table 1 and chapter 2.2), but at a considerably higher field than that of **1** (δ = 224.5 ppm in C₆D₆).² The

$^1J(^{29}\text{Si}, ^1\text{H})$ (204.2 Hz) and $^2J(^{29}\text{Si}, ^1\text{H})$ (14.8 Hz) coupling constants compare well with those of the 1,2-dihydridodisilenes (*E*)- $\text{Si}_2\text{H}_2\text{R}_2$ ($\text{R} = \text{Bbp}$, Bbt ; $^1J(^{29}\text{Si}, ^1\text{H}) = 216$ Hz and 210 Hz, respectively; $^2J(^{29}\text{Si}, ^1\text{H}) = 16$ Hz in both compounds),³⁰ indicating an increased s-character of the Si hybrid orbital involved in the Si–H bond in full agreement with the NBO analysis results of **1H**⁺ (see SI, Table S8).

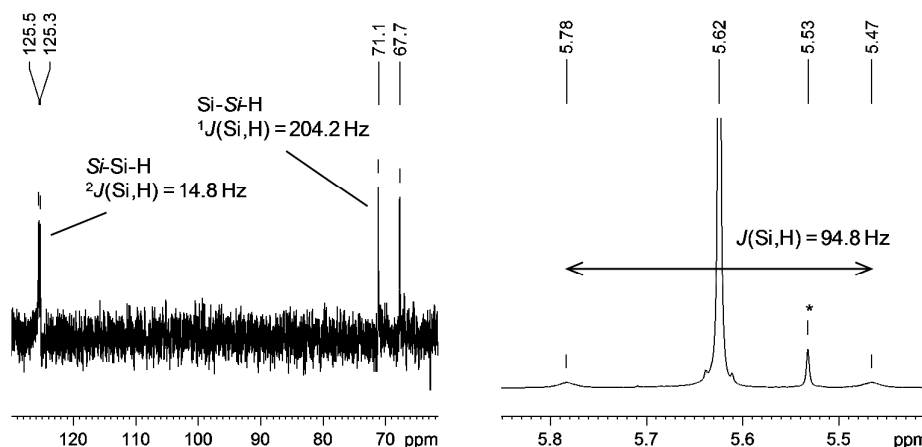


Figure 2. Left: ^{29}Si NMR spectrum of **1H**[$\text{B}(\text{Ar}^{\text{F}})_4$] at 213 K displaying two doublets with characteristic $^1J(^{29}\text{Si}, ^1\text{H})$ and $^2J(^{29}\text{Si}, ^1\text{H})$ coupling constants. Right: Excerpt of the ^1H NMR spectrum of **1H**[$\text{B}(\text{Ar}^{\text{F}})_4$] at 25 °C displaying the Si–H resonance at $\delta = 5.62$ ppm with a mean $J(^{29}\text{Si}, ^1\text{H})$ coupling constant due to the positional exchange of the Si sites; the signal marked with an asterisk originates from a small amount of an unknown impurity.

Additional evidence for the dynamic process was provided by the slow exchange limit ^1H and $^{13}\text{C}\{^1\text{H}\}$ spectra of **1H**[$\text{B}(\text{Ar}^{\text{F}})_4$] ($\text{THF}-d_8$, 213 K), which display a double set of signals for the heterotopic Idipp substituents, whereas the fast exchange limit ^1H and $^{13}\text{C}\{^1\text{H}\}$ spectra of **1H**[$\text{B}(\text{Ar}^{\text{F}})_4$] ($\text{THF}-d_8$, 333 K) reveal only one set of signals (see SI, Figures S2 – S7). The number and relative intensities of the Idipp signals in the slow exchange ^1H and $^{13}\text{C}\{^1\text{H}\}$ NMR spectra clearly indicate that both NHC groups rotate fast about the Si– C_{NHC} bonds on the NMR time scale. Most distinctive are the signals of the C_{NHC} nuclei in the $^{13}\text{C}\{^1\text{H}\}$ NMR spectra (Table 1). The signal of the Si1-bonded C_{NHC} atom appears at lower frequency ($\delta = 161.8$ ppm) than that of the Si2-bonded C_{NHC} atom ($\delta = 174.5$ ppm), and both C_{NHC} atoms have a chemical shift in between that of Idipp ($\delta = 220.6$ ppm in C_6D_6)³³ or **1** ($\delta = 196.3$ in C_6D_6)² and the imidazolium salt (IdippH)Cl ($\delta = 139.3$ ppm in $\text{DMSO}-d_6$).^{5b} The same trend is observed for **1Me**[$\text{B}(\text{Ar}^{\text{F}})_4$] and **1Et**[$\text{B}(\text{Ar}^{\text{F}})_4$] and suggests a higher “imidazolium character” of the Si1-bonded NHC ring than that of the Si2-bonded NHC in **1R**[$\text{B}(\text{Ar}^{\text{F}})_4$] ($\text{R} = \text{H}$, Me , Et) (Table 1).

Topomerisation of **1H**[$\text{B}(\text{Ar}^{\text{F}})_4$] involves an intramolecular 1,2-H migration and proceeds according to quantum chemical calculations (chapter 2.3) via an NHC-stabilized disilahydronium intermediate (Scheme 2). Evidence for the intramolecularity of the process

was provided by the ^{29}Si satellite signals of the Si- H resonance in the ^1H NMR spectrum of $\mathbf{1H}[\text{B}(\text{Ar}^{\text{F}})_4]$ in $\text{THF-}d_8$ at 298 K ($\delta = 5.62$ ppm), which displays an averaged $J(^{29}\text{Si}, ^1\text{H})$ coupling constant of 94.8 Hz (Figure 2, right).³⁴ A similar topomerisation process has been proposed by G. Robinson et al. for the copper complex $[\text{CuCl}(\eta^1\text{-}\mathbf{1})]$, however without unambiguous experimental verification.^{22a} Furthermore, recent studies in our group have shown that the cation $[(\text{Idipp})(\text{I})\text{Si}=\text{Si}(\text{Idipp})]^+$ and the coinage metal complexes $[\text{MCl}(\eta^1\text{-}\mathbf{1})]$ and $[\text{M}(\eta^1\text{-}\mathbf{1})(\text{PMe}_3)][\text{B}(\text{Ar}^{\text{F}})_4]$ ($\text{M} = \text{Cu}, \text{Ag}, \text{Ag}$) undergo the same intramolecular topomerisation process in solution as observed for $\mathbf{1H}[\text{B}(\text{Ar}^{\text{F}})_4]$.^{4,22b-d}

The thermodynamic parameters of the topomerisation were obtained by full line-shape analysis of the NHC backbone $\text{C}^{4,5}\text{-}H$ ring proton signals in the temperature range of 213 – 273 K and were found to be $\Delta H^\ddagger = 38.5(\pm 2.4) \text{ kJ mol}^{-1}$ and $\Delta S^\ddagger = -54.3(\pm 7.7) \text{ J K}^{-1} \text{ mol}^{-1}$ (see SI, chapter 3). Remarkably, the Gibbs energy of activation ΔG^\ddagger ($51.6(\pm 0.6) \text{ kJ mol}^{-1}$ at $T_c = 241 \text{ K}$, $T_c =$ coalescence temperature) compares well with that calculated for the isomerization of the *trans*-bent disilene Si_2H_4 into the mono-hydrogen-bridged minimum structure (59 kJ mol^{-1}),³⁵ and the entropy of activation of the topomerisation of $\mathbf{1H}[\text{B}(\text{Ar}^{\text{F}})_4]$ is similar to that found for the intramolecular 1,2-hydrogen migration of the 1,2-dihydridodisilene (*E*)- $\text{Si}_2\text{H}_2\text{Bbt}_2$ ($-63(8) \text{ J K}^{-1} \text{ mol}^{-1}$), which leads via a silylsilylene intermediate to a silane.³⁰

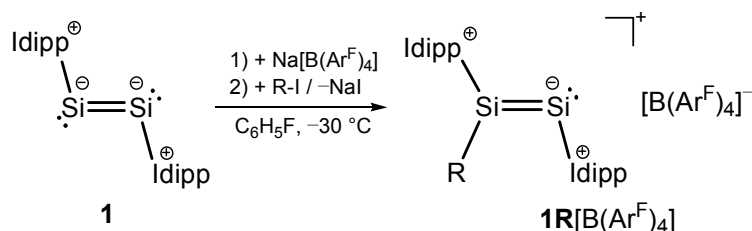
The topomerization of $\mathbf{1H}[\text{B}(\text{Ar}^{\text{F}})_4]$ is the first example of a reversible 1,2-hydrogen migration observed along a Si=Si bond in a molecular system and provides a molecular model for the migration of hydrogen atoms on Si(001) surfaces via “dangling bonds” (i.e. coordinatively unsaturated silicon centers),³⁶ which is suggested to account for the decrease in efficiency of photovoltaic cells based on hydrogenated amorphous silicon (Staebler-Wronski effect).³⁷ Topomerization of $\mathbf{1H}[\text{B}(\text{Ar}^{\text{F}})_4]$ is reminiscent of that of diazenium ions in acidic solutions, which has been suggested to proceed either via an intra- or intermolecular H^+ transfer,³⁸ and of the degenerate rearrangement of carbenium ions formed upon protonation of olefins.³⁹

Table 1: Comparison of selected NMR data of the cations $\mathbf{1R}^+$ in $\mathbf{1R}[\text{BAr}_4]$ ($\text{R} = \text{H}, \text{Me}, \text{Et}, \text{Na}; \text{Ar} = \text{Ar}^{\text{F}}; \text{R} = \text{I}, \text{Li}; \text{Ar} = \text{C}_6\text{F}_5$) and $\mathbf{1}$.

	$\delta(^{29}\text{Si})$ [ppm]		$\delta(\text{C}_{\text{NHC}})$ [ppm]	
	Si1	Si2	$\text{C}_{\text{NHC-Si1-R}}$	$\text{C}_{\text{NHC-Si2}}$
$\mathbf{1H}^+$	69.4 ^[c]	125.4 ^[c]	161.8 ^[c]	174.5 ^[c]
$\mathbf{1Me}^+$	102.8 ^[d]	115.2 ^[d]	162.9 ^[d]	177.1 ^[d]
	103.0 ^[e]	117.1 ^[e]		
$\mathbf{1Et}^+$	111.6 ^[d]	87.2 ^[d]	164.2 ^[d]	176.1 ^[d]
$\mathbf{1I}^{+[\text{a}]}$	-26.4 ^[f]	75.3 ^[f]	153.6 ^[f]	172.2 ^[f]
$\mathbf{1Li}^+$	301.1 ^[g]	301.1 ^[g]	188.8 ^[g]	188.8 ^[g]
$\mathbf{1Na}^+$	288.8 ^[g]	288.8 ^[g]	189.1 ^[g]	189.1 ^[g]
$\mathbf{1}^{[\text{b}]}$	224.5 ^[h]	224.5 ^[h]	196.3 ^[h]	196.3 ^[h]

[a]: Data taken from ref. [4]. [b]: Data taken from ref. [2]. [c]: $\text{THF-}d_8$, 213 K. [d]: $\text{THF-}d_8$, 298 K. [e]: $\text{C}_6\text{H}_5\text{F}$, 298 K [f]: $\text{THF-}d_8$, 203 K. [g]: $\text{C}_6\text{D}_5\text{Cl}$, 298 K. [h]: C_6D_6 , 298 K.

2.2 Alkylation of (Idipp)Si=Si(Idipp). Electrophilic alkylation of **1** was achieved upon treatment of **1** with the corresponding iodoalkane in the presence of Na[B(Ar^F)₄] to afford the mixed-valent alkyldisilicon(I) borates [(Idipp)(R)Si^{II}=Si^I(Idipp)][B(Ar^F)₄] (**1R**[B(Ar^F)₄], R = Me, Et) (Scheme 3). Remarkably, addition of Na[B(Ar^F)₄] to a solution of **1** in fluorobenzene led to a color change from dark red to brown to afford selectively the alkali metal disilicon(0) borate [Si₂(Na)(Idipp)₂][B(Ar^F)₄] (**1Na**[B(Ar^F)₄]) as discussed in chapter 2.4 (*vide infra*). Subsequent addition of the iodoalkane to the solution of **1Na**[B(Ar^F)₄] in fluorobenzene was accompanied by a color change from brown to bright orange and precipitation of NaI leading selectively to the alkyldisilicon(I) borate salts **1R**[B(Ar^F)₄] (Scheme 3). Remarkably, preactivation of **1** via complexation of Na[B(Ar^F)₄] is not indispensable for the formation of the alkyldisilicon(I) cations **1R**⁺, as evidenced by the reaction of **1** with iodomethane in C₆H₅F, which affords the analogous iodide salt [(Idipp)(Me)Si=Si(Idipp)]I according to ²⁹Si NMR spectroscopy. The salts **1R**[B(Ar^F)₄] were isolated after crystallization from fluorobenzene / *n*-hexane mixtures at -30 °C as highly air-sensitive, orange solids in moderate yields (R = Me: 36 %, R = Et: 50 %) (see SI, chapters 2.3 and 2.4). Notably, **1** did not react with 2-iodopropane indicating that bulky electrophiles cannot access the sterically protected Si₂ core of **1**. The compounds **1R**[B(Ar^F)₄] are thermally robust and decompose upon melting in vacuum-sealed glass capillaries at elevated temperatures (R = Me: 213 °C, R = Et: 209 °C). As in the case of **1H**[B(Ar^F)₄], the salts **1R**[B(Ar^F)₄] decompose slowly in THF-*d*₈ solution at ambient temperature, the decomposition leading to [IdippH][B(Ar^F)₄] and other unidentified products.



Scheme 3. Electrophilic alkylation of **1** to give the compounds **1R**[B(Ar^F)₄] (R = Me, Et). Formal charges are encircled.

Single-crystal X-ray diffraction analyses of **1Me**[B(Ar^F)₄] and **1Et**[B(Ar^F)₄] revealed that these compounds are isotypic with **1H**[B(Ar^F)₄]. The cations **1R**⁺ are well separated from the borate anions as evidenced by the shortest Si...F distances of 5.416(5) Å (**1Me**⁺) and 5.030(9) Å (**1Et**⁺) (cf. $\Sigma r(\text{Si}\cdots\text{F})_{\text{vdW}} = 3.6$ Å),²⁵ and reveal similar structural features as **1H**⁺, i.e. a *trans*-bent planar C_{NHC}-Si-Si-C_{NHC} core, in which a trigonal-planar coordinated Si1 atom (sum of angles at Si1: 359.6(1)° (**1Me**⁺), 359.9(2)° (**1Et**⁺)) is connected via a Si=Si bond to a V-shaped coordinated Si2 atom with a narrow angle at the Si2 atom (C28-Si2-Si1: 95.13(6)° (**1Me**⁺), 100.08(7)° (**1Et**⁺)) (Figure 3, Figure S34 (SI), Table 2). The Si-R (Si1-C56) bond lengths (**1Me**⁺: 1.885(2) Å, **1Et**⁺: 1.893(2) Å) are typical of Si-C single bonds and only slightly

shorter than the Si1–C_{NHC} bond lengths (**1Me**⁺: 1.901(2) Å, **1Et**⁺: 1.912(2) Å). Whereas the Si2-bonded central ring of the NHC group adopts in all cases an almost orthogonal orientation with respect to the planar C_{NHC}–Si–Si–C_{NHC} core of the cations ($\varphi_{\text{NHC2}} = 71.06(6)^\circ$ (**1H**⁺), 79.11(7)° (**1Me**⁺), 88.03(7)° (**1Et**⁺)),²⁶ the increasing bulkiness of the Si1-bonded substituent R in the series **1H**⁺ → **1Me**⁺ → **1Et**⁺ provokes a conformational change of the Si1-bonded NHC substituent from an almost coplanar orientation in **1H**⁺ ($\varphi_{\text{NHC1}} = 8.60(6)^\circ$) and **1Me**⁺ ($\varphi_{\text{NHC1}} = 13.23(8)^\circ$) to a synclinal conformation in **1Et**⁺ ($\varphi_{\text{NHC1}} = 52.52(8)^\circ$). The increased steric bulk of the R group can also be invoked to rationalize the gradual elongation of the Si1–C1 bonds in the series **1H**⁺ (1.882(2) Å) → **1Me**⁺ (1.901(2) Å) → **1Et**⁺ (1.912(2) Å) and the decrease of the C1–Si1–Si2 angles in the same series (**1H**⁺ (116.73(7)°) → **1Me**⁺ (114.62(7)°) → **1Et**⁺ (108.36(7)°)) (Table 2).

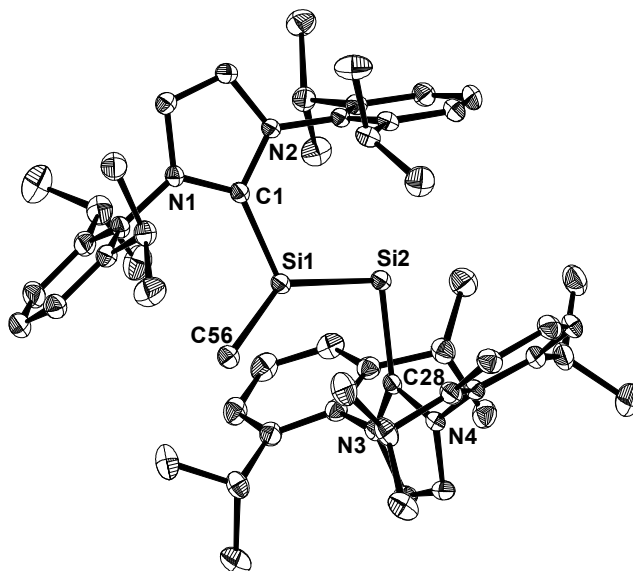


Figure 3. DIAMOND plot of the molecular structure of the cation **1Me**⁺ in the crystal lattice of **1Me**[B(Ar^F)₄] at 123(2) K. Thermal ellipsoids are set at 30 % probability. Hydrogen atoms were omitted for clarity. Selected bond lengths [Å], bond angles [°] and torsion angles [°]: Si1–C1 1.901(2), Si1–Si2 2.1909(8), Si2–C28 1.947(2), Si1–C56 1.885(2); C1–Si1–Si2 114.62(7), C1–Si1–C56 111.3(1), Si2–Si1–C56 133.71(8), C28–Si2–Si1 95.13(6); C1–Si1–Si2–C28 –177.4(1), C28–Si2–Si1–C56 10.7(1).

In contrast to **1H**[B(Ar^F)₄], multinuclear NMR spectroscopic studies of **1R**[B(Ar^F)₄] (R = Me, Et) in THF-*d*₈ indicate that no degenerate isomerization (topomerization) of the “σ-bonded” isomers occurs in solution up to 333 K.⁴⁰ Thus, the ¹H and ¹³C{¹H} NMR spectra display a double set of signals for the heterotopic *Idipp* substituents (see SI, Figures S12 – S15 and S17 – S21), which could be unequivocally assigned by a combination of ¹H–¹³C HMQC, ¹H–¹³C HMBC and ¹H–²⁹Si HMBC correlation spectroscopies using the correlation between the C^{4,5}-H proton signals of the NHCs and the ²⁹Si NMR signals. The number and relative

intensity of the signals of each Idipp group indicates that both NHCs rotate fast about the respective Si–C_{NHC} bonds on the NMR time scale. Similarly, the ²⁹Si NMR spectra of **1R**[B(Ar^F)₄] (R = Me, Et) in THF-*d*₈ show two separate resonances at 298 K (Table 1), which were unequivocally assigned by two-dimensional ¹H-²⁹Si HMBC spectroscopy. The ²⁹Si NMR spectrum of **1Me**[B(Ar^F)₄] was also recorded in C₆H₅F and displayed two signals at 103.0 and 117.1 ppm (calibrated against SiMe₄), i.e. at almost the same position as those observed in THF-*d*₈ (102.8 and 115.2 ppm, respectively) (Table 1). This observation excludes a coordination of THF to the potentially electrophilic Si2-center of the cations [(Idipp)(Me)Si=Si(Idipp)]⁺ in solution. Moreover, the ²⁹Si NMR chemical shifts of the corresponding iodide salt **1Me**[I] in C₆H₅F (103.5 and 112.6 ppm) are quite similar to those of **1Me**[B(Ar^F)₄] suggesting a negligible interaction of the stronger nucleophile I[−] with **1Me**⁺.

A comparison of the ²⁹Si NMR chemical shifts of **1R**⁺ reveals, that the three-coordinated Si nuclei (Si-R) are progressively deshielded in the series **1H**[B(Ar^F)₄] (δ = 69.4 ppm) → **1Me**[B(Ar^F)₄] (δ = 102.8 ppm) → **1Et**[B(Ar^F)₄] (δ = 111.6 ppm) (Table 1). Notably, a similar, however less pronounced trend is observed in the series of the alkyl silanes SiMe₃R upon replacement of the R substituent (H (δ = −18.5 ppm) → Me (δ = 0.0 ppm) → Et (δ = 1.6 ppm)).⁴¹ In comparison, the two-coordinated ²⁹Si NMR nuclei are progressively shielded in the same series **1H**[B(Ar^F)₄] (δ = 125.4 ppm) → **1Me**[B(Ar^F)₄] (δ = 115.2 ppm) → **1Et**[B(Ar^F)₄] (δ = 87.2 ppm) (Table 1). Remarkably, a similar influence of the substituents R was observed on the ¹³C NMR chemical shifts of the C^α and C^β atoms in the alkenes R-C^βH=C^αH₂ (R = H, Me, Et).⁴²

Table 2: Comparison of selected bond lengths [Å], bond angles [°] and dihedral angles [°] of the cations **1R**⁺ in **1R**[BAr₄] (R = H, Me, Et, Na; Ar = Ar^F; R = I, Li; Ar = C₆F₅) and **1**.

	Si–Si [Å]	Si1–C _{NHC} [Å]	Si2–C _{NHC} [Å]	C _{NHC} –Si1–Si2 [°]	C _{NHC} –Si2–Si1 [°]	φ _{NHC1} ^[a] [°]	φ _{NHC2} ^[a] [°]
1H ⁺	2.1873(8)	1.882(2)	1.940(2)	116.73(7)	95.34(6)	8.60(6)	71.06(6)
1Me ⁺	2.1909(8)	1.901(2)	1.947(2)	114.62(7)	95.13(6)	13.23(8)	79.11(7)
1Et ⁺	2.1726(9)	1.912(2)	1.941(2)	108.36(7)	100.08(7)	52.52(8)	88.03(7)
1I ⁺ [b]	2.1739(9)	1.901(2)	1.931(2)	112.83(7)	96.61(7)	96.69(7)	95.78(7)
1Li ⁺	2.234(1)	1.941(3)	1.938(3)	94.9(1)	98.7(1)	79.0(1)	108.9(1)
1Na ⁺	2.248(2)	1.948(4)	1.948(4)	95.4(1)	95.4(1)	87.7(1)	87.7(1)
1 ^[c]	2.229(1)	1.927(2)	1.927(2)	93.37(5)	93.37(5)	87.11(5)	87.11(5)

[a]: φ_{NHC1} and φ_{NHC2} are the dihedral angles between the least-square plane of the C_{NHC}–Si–Si–C_{NHC} atoms and the Si1- and Si2-bonded NHCs rings, respectively. [b]: Data taken from ref. [4]. [c]: Data taken from ref. [2].

2.3 Quantum chemical studies of 1H^+ and 1Me^+ . In order to get a closer insight into the topomerisation of 1H^+ , the energy hypersurface of 1H^+ was analyzed and compared with that of 1Me^+ by quantum chemical calculations at the B97-D3 level of theory,^{43a-d} including the COSMO solvation model^{43e} and RI-JCOSX approximations (see SI, chapter 5).^{43f,g} The def2-TZVP basis sets were used for the Si, N, heterocyclic C atoms and the Si1-attached H atom and methyl group, and the def2-SVP basis sets for all peripheral carbon and all other hydrogen atoms.^{43h,i} The level of theory is abbreviated in the following as B97-D3/I.

Geometry optimization of 1H^+ and 1Me^+ afforded minimum structures with a Si1–H and Si1–Me σ -bond (“ σ -bonded” isomers),⁴⁴ which are designated in the following as $1\text{H}^+_{\text{calc}}$ and $1\text{Me}^+_{\text{calc}}$. A comparison of the structural parameters revealed an excellent agreement between the calculated and the experimental bond lengths and angles obtained for $1\text{H}[\text{B}(\text{Ar}^{\text{F}})_4]$ and $1\text{Me}[\text{B}(\text{Ar}^{\text{F}})_4]$ by X-ray crystallography. Remarkably, also the quite different conformation of the Si1-bonded NHC compared to the Si2-bonded NHC could be well reproduced by the quantum chemical calculations (see SI, Tables S4 and S5).

A second minimum structure could be localized on the energy hypersurface of 1H^+ and 1Me^+ , which is however less stable than that of $1\text{H}^+_{\text{calc}}$ and $1\text{Me}^+_{\text{calc}}$ by 30.5 kJ mol^{-1} and 95.4 kJ mol^{-1} (ΔG values at 298 K), respectively. $(1\text{H}^+)'_{\text{calc}}$ features a “symmetric” H-bridged structure, in which the H atom is located over the Si–Si bond at almost the same distance from the two Si atoms (“ π -bonded” isomer).⁴⁴ Notably, the Si–Si bond of $(1\text{H}^+)'_{\text{calc}}$ (2.301 Å) is longer than the Si=Si bond of $1\text{H}^+_{\text{calc}}$ (2.198 Å), and its length approaches the Si–Si single bond length in α -Si (2.352 Å).⁴⁵ $(1\text{H}^+)'_{\text{calc}}$ features a 3c-2e Si–H–Si interaction, which leads to longer Si–H bonds (1.716 and 1.710 Å) than the 2c-2e Si–H bond (1.486 Å) of $1\text{H}^+_{\text{calc}}$ (“ σ -bonded” isomer). The two minimum structures are connected via a transition state $(1\text{H}^+)_{\text{calc}}^{\text{TS}}$, which lies 42.9 kJ mol^{-1} higher in energy than $1\text{H}^+_{\text{calc}}$ (Figure 4). The calculated barrier agrees acceptably well with the experimentally derived Gibbs energy of activation ($\Delta G^\ddagger(298 \text{ K}) = 54.7 \pm 0.2 \text{ kJ mol}^{-1}$). The conversion of $1\text{H}^+_{\text{calc}}$ to $(1\text{H}^+)'_{\text{calc}}$ involves a H-migration from the end-on to a bridging position and a concomitant rotation of the Si1-bonded heterocyclic ring from an almost coplanar orientation in $1\text{H}^+_{\text{calc}}$ ($\varphi_{\text{NHC1}} = 3.63^\circ$) to an almost orthogonal orientation in $(1\text{H}^+)'_{\text{calc}}$ ($\varphi_{\text{NHC1}} = 76.17^\circ$) (see SI, Table S4).²⁶

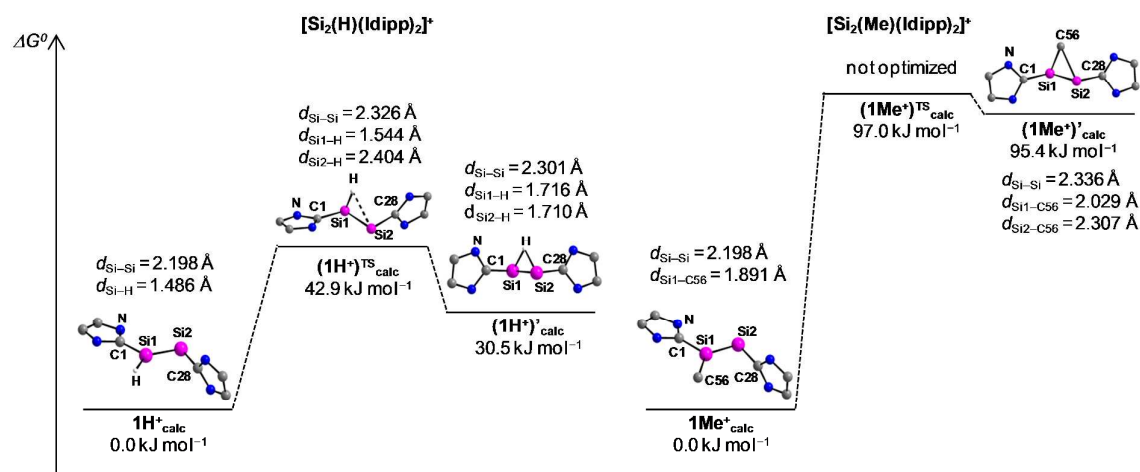


Figure 4. Schematic Gibbs profiles ($T = 298 \text{ K}$) for the degenerate isomerizations of $[\text{Si}_2(\text{H})(\text{ldipp})_2]^+$ (left) and $[\text{Si}_2(\text{Me})(\text{ldipp})_2]^+$ (right) which includes the optimized minimum structures $1\text{H}^+_{\text{calc}}$, $1\text{Me}^+_{\text{calc}}$, $(1\text{H}')_{\text{calc}}$ and $(1\text{Me}')_{\text{calc}}$ and the transition state $(1\text{H}^+)_{\text{calc}}^{\text{TS}}$ with selected bonding parameters. The N-bonded dipp substituents and H atoms, except the Si-bonded H atom, were omitted for clarity and only one half of the symmetric energy profiles is depicted.

In contrast to $(1\text{H}')_{\text{calc}}$, the second minimum structure ($(1\text{Me}')_{\text{calc}}$) located on the energy hypersurface of 1Me^+ reveals an asymmetric bridging of the Si–Si single bond (2.336 \AA) by the methyl group, as evidenced by the markedly different Si1–C56 (2.029 \AA) and Si2–C56 (2.307 \AA) bonds (Figure 4). Both Si–C_{Me} bonds are longer than the 2c-2e Si–C_{Me} bond of the “ σ -bonded” isomer $1\text{Me}^+_{\text{calc}}$ (1.891 \AA). A relaxed potential energy surface scan of 1Me^+ was performed starting from $1\text{Me}^+_{\text{calc}}$, which involved a progressive decrease of the Si2–C_{Me} distance from 377 pm (the Si2–C_{Me} distance in $1\text{Me}^+_{\text{calc}}$) to 137 pm in 12 steps. This scan afforded a maximum, which displayed one imaginary frequency of -177 cm^{-1} and a Gibbs energy of 97 kJ mol^{-1} . Further optimization of this maximum structure did not furnish the transition state $(1\text{Me}^+)_{\text{calc}}^{\text{TS}}$, but instead led to the minimum structures $1\text{Me}^+_{\text{calc}}$ and $(1\text{Me}')_{\text{calc}}$ indicating a flat progression of the potential energy surface during interconversion of $(1\text{Me}')_{\text{calc}}$ into the overall minimum structure $1\text{Me}^+_{\text{calc}}$ (Figure 4). The significantly higher energy barrier for the transformation of $1\text{Me}^+_{\text{calc}}$ into $(1\text{Me}')_{\text{calc}}$ compared to that of 1H^+ confirms the observed rigidity of 1Me^+ on the NMR timescale.

NBO (natural bond orbital) analyses of the “ σ -bonded” isomers $1\text{H}^+_{\text{calc}}$ and $1\text{Me}^+_{\text{calc}}$ revealed a localized Si1–R ($R = \text{H}, \text{Me}$) σ -bond NBO, a Si–Si σ - and π -bond NBO, which are both polarized towards the Si1 atom, and a lone pair of electrons at Si2 in a natural hybrid orbital (NHO) with high s-character (ca. 77%) (see SI, Tables S8 and S10).^{43j} The rather high Wiberg bond Index (WBI) of the Si=Si bond of 1.61 ($1\text{H}^+_{\text{calc}}$) and 1.62 ($1\text{Me}^+_{\text{calc}}$) and the high covalent contribution to the overall NRT (natural resonance theory) Si–Si bond order of 1.85 ($1\text{H}^+_{\text{calc}}$) and 1.84 ($1\text{Me}^+_{\text{calc}}$) provide additional support for the presence of a slightly polar, covalent Si=Si bond.

Natural population analyses of $\mathbf{1H^+_{calc}}$ and $\mathbf{1Me^+_{calc}}$ revealed a considerable electron transfer from $\mathbf{1}$ to the electrophile (H^+ , Me^+), leading to a negative partial charge at the H atom ($q = -0.14e$) and the methyl group ($q = -0.38e$). The charge flow occurs mainly from the Si atoms, as evidenced by a comparison of the Si partial charges in $\mathbf{1H^+_{calc}}$ ($q(Si1) = 0.31e$, $q(Si2) = 0.26e$) and $\mathbf{1Me^+_{calc}}$ ($q(Si1) = 0.65e$, $q(Si2) = 0.20e$) with those in $\mathbf{1_{calc}}$ ($q(Si1, Si2) = -0.10e$) (see SI, Tables S7, S8 and S10).

In comparison, the “ π -bonded” isomers $(\mathbf{1H^+})'_{calc}$ and $(\mathbf{1Me^+})'_{calc}$ display only one non-polarized NBO corresponding to the Si–Si σ -bond, with each Si atom carrying a lone pair of electrons in a NHO with high s-character (see SI, Tables S9 and S11). This leads to a considerably lower Si–Si WBI ($(\mathbf{1H^+})'_{calc}$: 1.01; $(\mathbf{1Me^+})'_{calc}$: 0.90) than those of $\mathbf{1H^+_{calc}}$ and $\mathbf{1Me^+_{calc}}$ and to a Si–Si NRT bond order ($(\mathbf{1H^+})'_{calc}$: 0.96; $(\mathbf{1Me^+})'_{calc}$: 0.90), which lies at half the value of that in the “ σ -bonded” isomers $\mathbf{1H^+_{calc}}$ and $\mathbf{1Me^+_{calc}}$. All these results suggest the presence of a Si–Si single bond in $(\mathbf{1H^+})'_{calc}$ and $(\mathbf{1Me^+})'_{calc}$.

The largest difference between $(\mathbf{1H^+})'_{calc}$ and $(\mathbf{1Me^+})'_{calc}$ exists with respect to the Si–R–Si interaction. In $(\mathbf{1H^+})'_{calc}$, a highly localized NBO is found corresponding to the 3c-2e Si–H–Si interaction, which is formed of an almost pure p NHO of each Si atom and the hydrogen 1s orbital and is polarized towards the H atom (Figure 5, left). In comparison, only a NBO for the $\sigma(Si1-C_{Me})$ bond, but no NBO for the Si2– C_{Me} bond was found in $(\mathbf{1Me^+})'_{calc}$ (see SI, Table S11). Instead, the Si2 atom bears a lone vacancy of pure p-character (with an occupancy of 0.26 electrons), which attains electron density from the $\sigma(Si1-C_{Me})$ and one $\sigma(C-H)$ orbital of the methyl group according to second order perturbation theory. The corresponding second order perturbation energies $E^{(2)}$ amount to $196.6 \text{ kJ mol}^{-1}$ and $156.9 \text{ kJ mol}^{-1}$, respectively. This “agostic-type” interaction locates one of the methyl hydrogen atoms ($H1$) in the Si2–Si1– $C56$ plane and leads to an elongation of one C_{Me} – $H1$ ($C56$ – $H1$) bond reducing the electron deficiency at the Si2 atom (Figure 5, right).

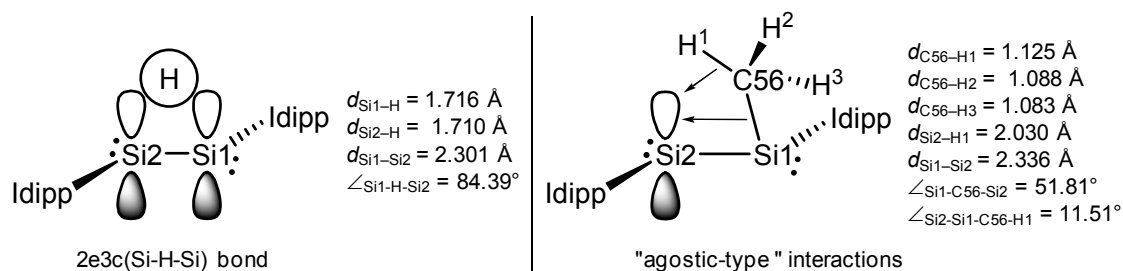
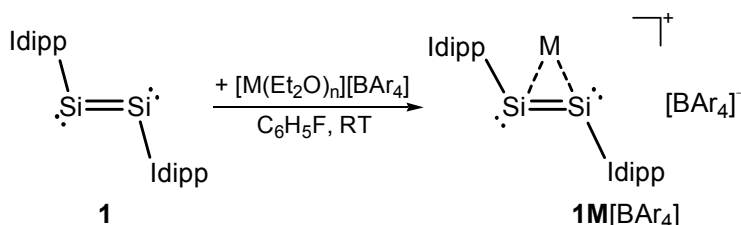


Figure 5. Left: Schematic presentation of the Si–R–Si interaction in the “ π -coordinated” isomers of $(\mathbf{1H^+})$ (left) and $\mathbf{1Me^+}$ (right) according to NBO analyses with selected bonding parameters.

2.4 Addition of alkali metal borates to (Idipp)Si=Si(Idipp). During the syntheses of $1\mathbf{R}[\mathbf{B}(\text{Ar}^{\text{F}})_4]$ ($\text{R} = \text{Me}, \text{Et}$) from **1**, $\text{Na}[\mathbf{B}(\text{Ar}^{\text{F}})_4]$ and RI , a color change of the dark red solution of **1** in $\text{C}_6\text{H}_5\text{F}$ to brown was observed upon treatment with $\text{Na}[\mathbf{B}(\text{Ar}^{\text{F}})_4]$. This stimulated us to study the interaction of **1** with alkali metal cations. In fact, compound **1** readily reacted with the alkali metal borates $[\text{Li}(\text{Et}_2\text{O})_{2.5}][\mathbf{B}(\text{C}_6\text{F}_5)_4]^{46}$ and $\text{Na}[\mathbf{B}(\text{Ar}^{\text{F}})_4]^{24b,47}$ to afford after crystallization from fluorobenzene / *n*-hexane mixtures the alkali metal disilicon(0)-borates $[\text{Si}_2(\text{M})(\text{Idipp})_2][\mathbf{BAr}_4]$ (**1M** $[\mathbf{BAr}_4]$; $\text{M} = \text{Li}, \text{Ar} = \text{C}_6\text{F}_5$; $\text{M} = \text{Na}, \text{Ar} = \text{Ar}^{\text{F}}$) as brown solids in 43 % ($\text{M} = \text{Li}$) and 70 % yield ($\text{M} = \text{Na}$), respectively (Scheme 4) (see SI, chapters 2.5 and 2.6). The compounds rapidly decompose upon contact with air, but are thermally quite robust solids (decomposition at 202 °C (**1Li** $[\mathbf{B}(\text{C}_6\text{F}_5)_4]$) and 211 – 212 °C (**1Na** $[\mathbf{B}(\text{Ar}^{\text{F}})_4]$)).



Scheme 4. Synthesis of the alkali metal disilicon(0)-borates **1M** $[\mathbf{BAr}_4]$ ($\text{M} = \text{Li}, \text{Ar} = \text{C}_6\text{F}_5, n = 2.5$; $\text{M} = \text{Na}, \text{Ar} = \text{Ar}^{\text{F}}, n = 0$). Formal charges and the η^6 -coordination of the two N-bonded dipp substituents are not depicted.

Dissolution of **1M** $[\mathbf{BAr}_4]$ ($\text{M} = \text{Li}, \text{Na}$) in coordinating solvents, such as diethyl ether or THF, led to an instant decomplexation of the alkali metal ions to give back **1** and the alkali metal borates. However, solutions of **1M** $[\mathbf{BAr}_4]$ in non-coordinating polar solvents (fluorobenzene, chlorobenzene) were found to be stable for several days at room temperature.

The solid state structures of **1Li** $[\mathbf{B}(\text{C}_6\text{F}_5)_4] \cdot (n\text{-C}_6\text{H}_{14})$ (Figure 6) and **1Na** $[\mathbf{B}(\text{Ar}^{\text{F}})_4]$ (see SI, Figure S35) were determined by single-crystal X-ray diffraction studies. The C_7 -symmetric cations **1Li** $^+$ and C_2 -symmetric cations **1Na** $^+$ are well separated from the borate counteranions, as apparent from the shortest $\text{Si} \cdots \text{F}$ distances of 6.155(3) Å and 6.809(6) Å, respectively (cf. $\sum r(\text{Si} \cdots \text{F})_{\text{vdW}} = 3.6$ Å).²⁵ The alkali metal cations are encapsulated in the cavity of the (Idipp)Si=Si(Idipp) core of **1Li** $^+$ and **1Na** $^+$ via η^2 -coordination to the Si=Si π -bond and η^6 -coordination to two peripheral 2,6-diisopropylphenyl (dipp) rings (Figure 6 and Figure S35 (SI)). The Si–Li bond distances in **1Li** $^+$ (Si1–Li: 2.822(6) Å, Si2–Li: 2.925(7) Å) are quite long and comparable to that of the contact ion pair $\text{R}_2\text{Si}=\text{Si}(\text{R})\text{Li}(\text{dme})_2$ (2.853(3) Å, $\text{R} = \text{C}_6\text{H}_2\text{-2,4,6-}i\text{Pr}_3$).⁴⁸ They suggest a weak $\text{Si} \cdots \text{Li}$ interaction, which is corroborated by the only slightly elongated Si=Si bond (2.234(1) Å, 0.2 %) compared to **1** (2.229(1) Å).² The Si–Na bond lengths in **1Na** $^+$ (3.096(3) Å) are similar to the Si–Na bond lengths in the dimer $(\text{NaSi}i\text{Bu}_3)_2$ (3.060(4) and 3.073(4) Å),⁴⁹ and the Si=Si bond (2.248(2) Å) of **1Na** $^+$ is slightly more elongated (0.9 %) than in **1Li** $^+$.

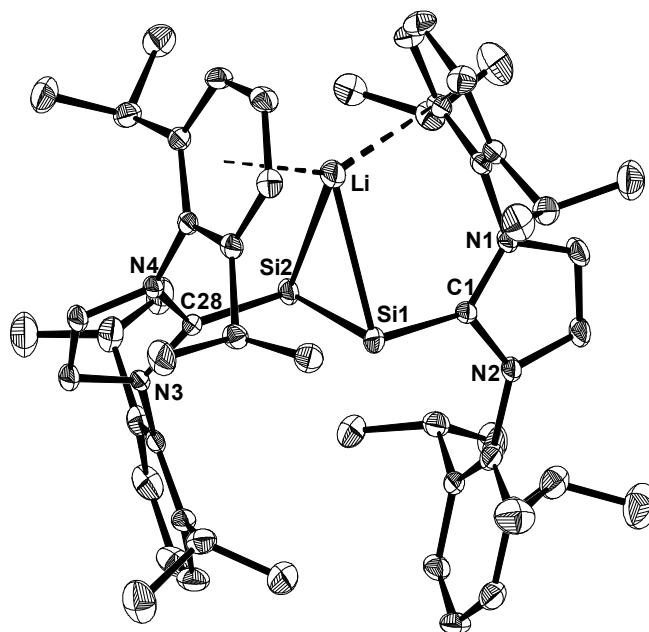


Figure 6. DIAMOND plot of the molecular structure of 1Li^+ in the crystal lattice of $1\text{Li}[\text{B}(\text{C}_6\text{F}_5)_4] \cdot (n\text{-C}_6\text{H}_{14})$ at 123(2) K. Thermal ellipsoids are set at 30 % probability. Hydrogen atoms were omitted for clarity. Selected bond lengths [Å], bond angles [°] and torsion angles [°]: C1–Si1 1.941(3), C28–Si2 1.938(3), Li–Si1 2.822(6), Li–Si2 2.925(7), Si1–Si2 2.234(1); Si1–Li–Si2 45.7(1), C1–Si1–Si2 94.9(1), C1–Si1–Li 95.9(2), Si2–Si1–Li 69.6(1), C28–Si2–Si1 98.7(1), C28–Si2–Li 93.7(2), Si1–Si2–Li 64.7(1); C1–Si1–Si2–C28 175.5(1).

Encapsulation of the Li^+ and Na^+ ions in the cavity of **1** leads only to minor structural changes of the (Idipp)Si=Si(Idipp) core (Table 1). This suggests a mainly electrostatic bonding of the alkali metal ions to the Si=Si π bond and the π -electron systems of the two dipp substituents, which is typical for alkali metal cation- π interactions.⁵⁰ Notably the M–arene_{centroid} distances (2.292 Å and 2.451 Å in 1Li^+ , 2.557 Å in 1Na^+), compare well with those of the alkali metal cation- π complexes $[\text{Li}(\eta^6\text{-toluene})][\text{CB}_{11}\text{Me}_{12}]$ (2.39, 2.45 Å) and $[\text{Na}(\eta^6\text{-benzene})_2][\text{CB}_{11}\text{Me}_{12}]$ (2.69 and 2.71 Å).⁵¹ Remarkably, a similar reaction of the diboron(0) compound (Idipp)B≡B(Idipp) with alkali metal borates was reported recently to give the cations $[\text{B}_2(\text{M})(\text{Idipp})_2]^+$ (M = Li, Na), which however could not be isolated and structurally characterized.⁵²

Multinuclear NMR spectroscopic analyses of $1\text{M}[\text{BAr}_4]$ in $\text{C}_6\text{D}_5\text{Cl}$ indicate clearly that the encapsulation of the alkali metal cations is retained in solution. Thus, the $^{29}\text{Si}\{^1\text{H}\}$ NMR spectrum of $1\text{Li}[\text{B}(\text{C}_6\text{F}_5)_4]$ displays one broadened signal at 301.1 ppm and that of $1\text{Na}[\text{B}(\text{Ar}^{\text{F}})_4]$ one sharp ^{29}Si NMR signal at 288.8 ppm (see SI, Figures S26 and S30). Both ^{29}Si NMR resonances appear at considerably lower field compared to **1** ($\delta = 224.5$ ppm).² Remarkably, the opposite trend was observed for the ^{29}Si NMR resonances of η^2 -disilene complexes of transition metals, which can be explained by the considerable metal-ligand π back-bonding in the latter compounds.⁵³ No coupling between the ^{29}Si ($I = 1/2$) and the

quadrupolar ${}^7\text{Li}$ ($I = 3/2$) nucleus could be resolved in the ${}^{29}\text{Si}\{{}^1\text{H}\}$ NMR spectrum of $\mathbf{1Li[B(C_6F_5)_4]}$ at 298 K and 243 K, due to signal broadening. However, the width of the ${}^{29}\text{Si}$ NMR signal of $\Delta\nu \approx 56$ Hz (298 K) suggests, that the upper limit of the scalar ${}^{29}\text{Si}$ - ${}^7\text{Li}$ coupling would be 14 Hz. This value is considerably smaller than those in lithiosilanes (${}^1J({}^{29}\text{Si}, {}^7\text{Li}) = 32.8 - 65.3$ Hz),⁵⁴ providing additional evidence for the mainly electrostatic interaction of the alkali metal ions with the Si=Si π -bond in $\mathbf{1M[Bar_4]}$. Notably, the ${}^7\text{Li}$ NMR signal of $\mathbf{1Li[B(C_6F_5)_4]}$ ($\delta = -6.7$ ppm) appears in the common range of π -complexated Li^+ ions,⁵⁵ but at considerably higher field than that of $[\text{Li}(\text{Et}_2\text{O})_{2.5}][\text{B(C}_6\text{F}_5)_4]$ ($\delta = -1.1$ ppm in $\text{C}_6\text{H}_5\text{F}$). This observation suggests a tight encapsulation of the Li^+ ion by $\mathbf{1}$ in solution.

The ${}^1\text{H}$ and ${}^{13}\text{C}$ NMR spectra of $\mathbf{1M[Bar_4]}$ display a single set of signals for the two Idipp substituents indicating that a rapid site exchange of the η^6 -coordinated dipp groups with those which are not bonded to the alkali metal ions occurs on the NMR time scale (see SI, Figures S23 – S25 and S27 – S29). No splitting of the ${}^1\text{H}$ NMR signals was observed at -40 °C just above the freezing point of $\text{C}_6\text{D}_5\text{Cl}$ (-45 °C). It is presently unclear whether this site exchange is an intramolecular process involving a successive or concomitant rotation of the NHC groups about the respective Si– C_{NHC} bonds. An intermolecular Li^+ exchange seems less probable given the broadening of the ${}^{29}\text{Si}$ NMR resonance induced by the unresolved spin-spin coupling.

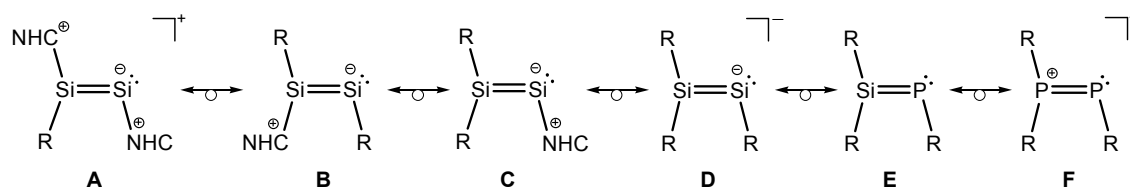
Quantum chemical calculations of the cation $\mathbf{1Li}^+$ were carried out on the B97-D3/I level of theory to analyze the interaction of Li^+ with the (Idipp)Si=Si(Idipp)₂ core of $\mathbf{1}$.⁴³ The structural parameters of the optimized minimum structure $\mathbf{1Li}^+_{\text{calc}}$ agree well with the experimental values (see SI, Table S6).

A look at the Kohn-Sham orbitals of $\mathbf{1Li}^+_{\text{calc}}$ revealed the same sequence of frontier orbitals as in $\mathbf{1}$, in which the $n_+(\text{Si-Si})$ orbital is the HOMO, the Si=Si π -orbital is the HOMO–1 and the $n_-(\text{Si-Si})$ orbital is the HOMO–2 (see SI, Figure S43).^{8,18} No orbitals pointing to an interaction between Li^+ and the η^2 -coordinated Si=Si bond or the η^6 -coordinated aryl substituents were found by the calculations due to the mainly electrostatic bonding of Li^+ , which was further confirmed by an NBO analysis of $\mathbf{1Li}^+_{\text{calc}}$ (see SI, Table S12). The Li atom displays a lone vacancy with a small occupancy of 0.13. Second order perturbation theory analysis of the Fock matrix in the NBO basis revealed only small interaction energies between the Si-based or aryl-based donor NBOs and the lone vacancy on the Li atom (see SI, Table S13), which is characteristic of electrostatic cation- π interactions.⁵⁶

Consequently, the encapsulation of the Li^+ cation in the cavity of $\mathbf{1}$ is accompanied by only a minor charge transfer to the Li^+ ion, which still carries a high positive charge in $\mathbf{1Li}^+_{\text{calc}}$ according to an NPA charge analysis ($q(\text{Li}) = 0.85e$). This charge transfer occurs exclusively from the NHCs, as evidenced by the essentially identical NPA charges of the Si atoms in $\mathbf{1Li}^+$

($q(\text{Si}1) = -0.12\text{e}$, $q(\text{Si}2) = -0.11\text{e}$) and in **1** ($q(\text{Si}1, \text{Si}2) = -0.10\text{e}$) (see SI, Tables S7 and S12).

2.5 Quantum chemical calculations of a series of isolobal compounds with $[(\text{Idipp})(\text{R})\text{Si}^{\text{II}}=\text{Si}^0(\text{Idipp})]^+$. Formal replacement of the $[\text{Si}(\text{Idipp})]$ fragments in $[(\text{Idipp})(\text{R})\text{Si}^{\text{II}}=\text{Si}^0(\text{Idipp})]^+$ (**1R**⁺, R = H, Me, Et) by the isolobal fragments $[\text{SiR}]^-$ and $[\text{PR}]^{19,20}$ leads to a series of Si and P multiple-bonded compounds **B – F**, which are depicted in Scheme 5. Class **B**,¹² **C**²⁷ and **F**^{23a} compounds are very rare, whereas disilenide anions (**D**)^{28,48,57} and phosphasilenes (**E**)⁵⁸ are familiar classes of compounds, the synthetic potential of which has been exploited. A comparison of **A** with **B – F** unraveled many common structural features, which stimulated us to study their electronic structures.



Scheme 5. Isolobal derivatives of the cations $[(\text{NHC})(\text{R})\text{Si}^{\text{II}}=\text{Si}^0(\text{NHC})]^+$ (**A**; **A** = **1R**⁺ for NHC = Idipp and R = H, Me, Et).

For this purpose quantum chemical calculations of the model systems with $\text{NHC}^{\text{Me}} = \text{C}[\text{N}(\text{Me})\text{CH}]_2$ and R = Me were carried out on the B97-D3/RI-JCOSX/def2-TZVP level of theory.⁴³ The optimized minimum structures are depicted in Figure 7 and selected bonding parameters are given in Table 3. The structures of compounds **A**, **C**, **D**, **E** and **F** are quite similar as evidenced by the similar Si–Si, Si–C_{NHC} and Si–C_{methyl} bond lengths, the similar C1–E1–E2, C2–E2–E1, C1–E1–C3 and C3–E1–E2 bond angles (E = Si or P), the planar geometry around the E1 atoms and the orthogonal orientation of the Si2-bonded NHC substituent in compounds **A** and **C** with respect to the C1–Si1–Si2–C2 plane. The structural parameters of compound **B** differ slightly from those of compounds **A** and **C**, which becomes apparent from the slight pyramidalization of the Si1 atom and the synclinal orientation of the Si1-bonded NHC substituent towards the C1–Si1–Si2–C2 plane.

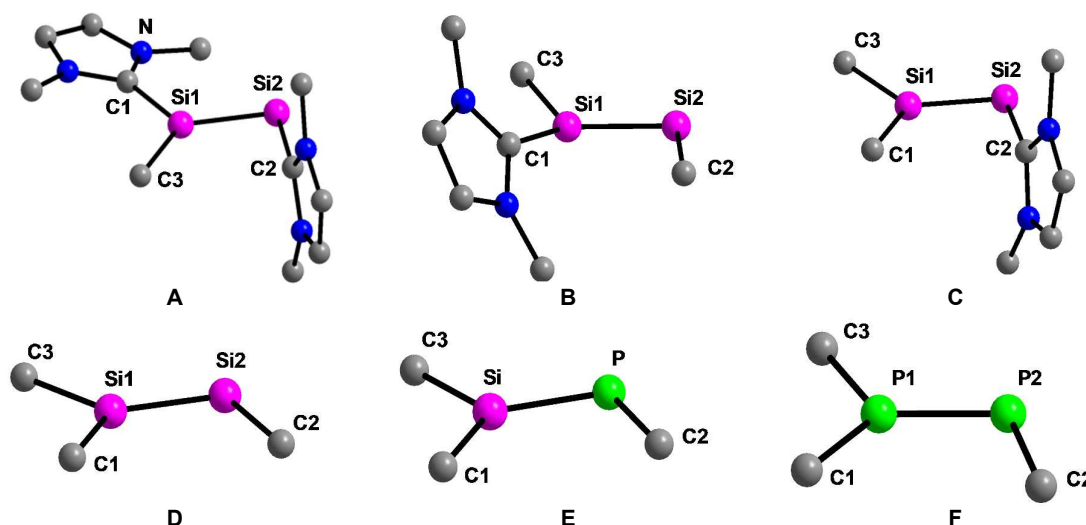


Figure 7. Calculated minimum structures of the model compounds **A** – **F** ($\text{NHC}^{\text{Me}} = \text{C}[\text{N}(\text{Me})\text{CH}]_2$, $\text{R} = \text{Me}$) depicted in Scheme 5. Hydrogen atoms were omitted for simplicity reasons.

Table 3: Selected calculated bond lengths, bond angles and dihedral angles of compounds **A** – **F** depicted in Figure 7; E = Si or P.

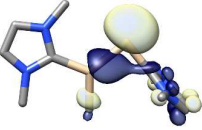
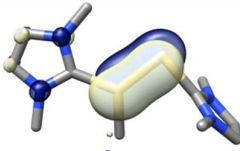
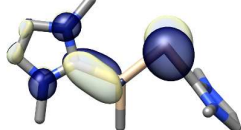
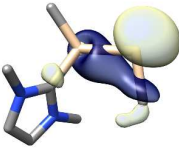
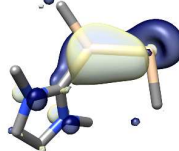
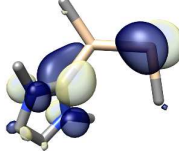
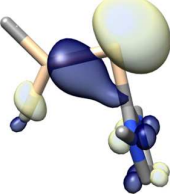
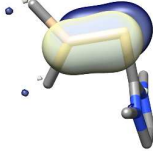
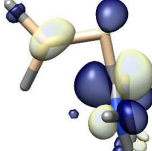
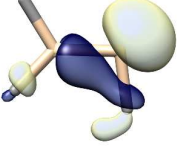
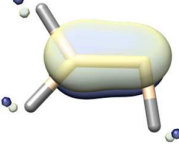
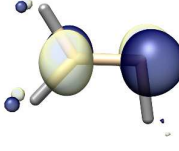
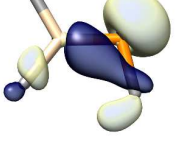
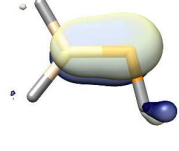
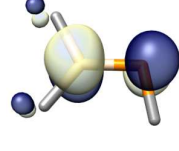
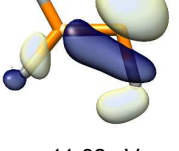
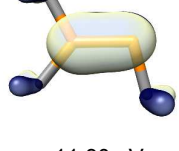
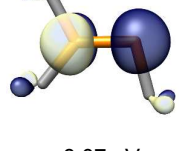
	E1–E2 [Å]	E1–C1 [Å]	E2–C2 [Å]	E1–C3 [Å]	C1–E1–E2 [°]	C2–E2–E1 [°]
A	2.213	1.890	1.946	1.900	118.45	89.50
B	2.240	1.882	1.962	1.911	121.59	101.14
C	2.192	1.910	1.931	1.900	129.55	88.91
D	2.210	1.935	1.997	1.927	132.00	99.53
E	2.083 ^[c]	1.885 ^[c]	1.889 ^[c]	1.881 ^[c]	129.14 ^[c]	102.08 ^[c]
F	2.010	1.812	1.850	1.807	130.06	104.02
	C1–E1–C3 [°]	C3–E1–E2 [°]	$\Sigma(\text{E1})^{\text{[a]}}$ [°]	$\varphi_{\text{NHC1}}^{\text{[b]}}$ [°]	$\varphi_{\text{NHC2}}^{\text{[b]}}$ [°]	
A	111.66	129.85	359.96	12.79	91.96	
B	109.06	124.43	355.08	53.23	–	
C	108.23	122.18	359.96	–	96.26	
D	104.95	123.05	360.00	–	–	
E	111.76 ^[c]	119.76 ^[c]	360.00 ^[c]	–	–	
F	112.80	117.14	360.00	–	–	

[a]: $\Sigma(\text{E1})$ is the sum of angles around the E1 atom. [b]: φ_{NHC1} and φ_{NHC2} are the dihedral angles between the least-square planes of the C1–E1–E2–C2 atoms and the heterocyclic ring atoms of the NHC substituents bonded to E1 and E2, respectively. [c]: E1 = Si, E2 = P.

A look at the Kohn-Sham orbitals of compounds **A** – **F** reveals the same sequence of frontier orbitals as expected for isolobal compounds (Table 4). Thus, the HOMOs are in all cases the E=E π -orbitals, the HOMOs–1 the lone pair orbitals at the two-coordinated E2 atoms (E2 = Si or P), and the LUMOs of compounds **A**, **B**, **D**, **E** and **F** the E=E π^* -orbitals. In the NHC-substituted compounds **A** and **B** a significant stabilization of the Si=Si π^* -orbital occurs via a bonding interaction with the C_{NHC} - and N_{NHC} -centered π^* -orbital of the NHC^{Me} -substituent. In compound **C** the Si=Si π^* -orbital is the LUMO+1, whereas the LUMO is mainly

the C_{NHC} - and N_{NHC} -centered π^* orbital of the Si2-bonded NHC-substituent. It is noteworthy that the Kohn-Sham orbitals of $1\text{H}^+_{\text{calc}}$, $1\text{Me}^+_{\text{calc}}$ (see SI, Figures S39 and S41), $[(\text{Idipp})(\text{I})\text{Si}=\text{Si}(\text{Idipp})]^+$,⁴ $\text{Tbb}(\text{Br})\text{Si}=\text{Si}(\text{SIIdipp})^{12}$ and the model compound $(\text{IMe}_4)(\text{R})\text{Si}=\text{SiR}$ ($\text{R} = \text{SiMe}_3$)²⁷ compare well those of the respective model systems depicted in Table 4.

Table 4: Selected Kohn-Sham orbitals and their energy eigenvalues of compounds **A** – **F** depicted in Figure 7; $\text{NHC}^{\text{Me}} = \text{C}[\text{N}(\text{Me})\text{CH}]_2$, $\text{R} = \text{Me}$. Isosurface value: 0.05 e Bohr⁻³.

	HOMO-1	HOMO	LUMO
$[(\text{NHC}^{\text{Me}})(\text{R})\text{Si}=\text{Si}(\text{NHC}^{\text{Me}})]^+ \text{ (A)}$	 -7.89 eV	 -7.23 eV	 -5.26 eV
$(\text{NHC}^{\text{Me}})(\text{R})\text{Si}=\text{SiR} \text{ (B)}$	 -3.95 eV	 -3.50 eV	 -1.73 eV
$\text{R}_2\text{Si}=\text{Si}(\text{NHC}^{\text{Me}}) \text{ (C)}$	 -4.34 eV	 -3.42 eV	 -1.06 eV
$[\text{R}_2\text{Si}=\text{SiR}]^- \text{ (D)}$	 0.30 eV	 0.94 eV	 3.54 eV
$\text{R}_2\text{Si}=\text{PR} \text{ (E)}$	 -5.76 eV	 -4.87 eV	 -1.70 eV
$[\text{R}_2\text{P}=\text{PR}]^+ \text{ (F)}$	 -11.82 eV	 -11.30 eV	 -8.07 eV

Whereas compounds **A** – **F** reveal the same number, symmetry properties and the same occupation of the frontier orbitals with electrons, the absolute energies of the frontier orbitals of **A** – **F** differ significantly (Table 4). This is not surprising given the different charges of the compounds and the considerable higher electronegativity of the [PR] than that of the [Si(NHC)] or [SiR][−] fragment, and implies a quite different reactivity of **A** – **F**, which remains to be exploited for the silicon compounds **A** – **C**. The interrelationship of **A** – **F** provides a different view of the bonding between NHCs and main-group elements from that developed by G. Frenking,¹⁴ and enables one to conceive many presently unknown Si compounds that are related to known phosphorus congeners.

3. Summary

The mixed-valent disilicon(I) borates **1R**[B(Ar^F)₄] (R = H, Me, Et) were obtained upon electrophilic addition of R⁺ to **1** and were comprehensively analyzed by a combination of structural, spectroscopic and quantum chemical methods. The unprecedented 1,2-hydrogen migration observed along the Si=Si bond of **1H**[B(Ar^F)₄] is reminiscent of the degenerate isomerization of carbenium ions, and can be considered as a molecular model for the H-migration in hydrogenated amorphous silicon that is of relevance in photovoltaics. The cations **1R**⁺ have considerable synthetic potential in silicon chemistry given their many potential reactivity sites, and can be strikingly viewed as NHC-trapped examples of the cations [Si₂R]⁺, providing another example for the exceptional ability of NHCs to stabilize low-valent silicon centers in unusual bonding environments. The interrelation of the electronic structure of the cations **1R**⁺ to those of a series of Si and P multiple-bonded compounds which are obtained upon replacement of the [Si(NHC)] by the isolobal [PR] and [SiR][−] fragments, provides a different view on the electronic structure of NHC-stabilized main-group element compounds. The Si⁰ compound **1** bears an optimal cavity for the complexation of alkali metal cations as demonstrated by the isolation and full characterization of **1M**[BAr₄] (M = Li, Na), which may become valuable reagents for the functionalization of **1** in reactions with main-group element or transition-metal halides.

Associated Content

Supporting Information

The supporting information (SI) contains the syntheses, analytical data and illustrations of the ¹H, ¹³C{¹H} and ²⁹Si{¹H} NMR spectra of **1H**[B(Ar^F)₄], **1Me**[B(Ar^F)₄], **1Et**[B(Ar^F)₄], **1Li**[B(C₆F₅)₄], and **1Na**[B(Ar^F)₄]. The SI also contains the analysis of the dynamic process of **1H**[B(Ar^F)₄] in solution as well as details of the quantum chemical calculations. This material is available

free of charge via the Internet at <http://pubs.acs.org>. Crystallographic data for **1H**[B(Ar^F)₄], **1Me**[B(Ar^F)₄], **1Et**[B(Ar^F)₄], **1Li**[B(C₆F₅)₄](*n*-C₆H₁₄) and **1Na**[B(Ar^F)₄] have been deposited with the Cambridge Structural Database under the deposition numbers CCDC 1448827 – 1448831.

Author Information

Corresponding Author

filippou@uni-bonn.de

Notes

The authors declare no competing financial interest.

Acknowledgements

We thank the Deutsche Forschungsgemeinschaft (SFB813, "Chemistry at Spin Centers") for financial support of this study. We also thank Dr. Ujjal Das and Dr. Senada Nozinovic for helpful discussions.

References

- (1) For recent reviews see: (a) Wang, Y.; Robinson, G. H. *Chem. Commun.* **2009**, 5201. (b) Wang, Y.; Robinson, G. H. *Dalton Trans.* **2012**, 41, 337. (c) Roesky, H. W. *J. Organomet. Chem.* **2013**, 730, 57. (d) Ghadwal, R. S.; Azhakar, R.; Roesky, H. W. *Acc. Chem. Res.* **2013**, 46, 444. (e) Wilson, D. J. D.; Dutton, J. L. *Chem. Eur. J.* **2013**, 19, 13626. (f) Martin, C. D.; Soleilhavoup, M.; Bertrand, G. *Chem. Sci.* **2013**, 4, 3020. (g) Wang, Y.; Robinson, G. H. *Inorg. Chem.* **2014**, 53, 11815. (h) Rivard, E. *Struct. Bond.* **2014**, 156, 203.
- (2) Wang, Y.; Xie, Y.; Wei, P.; King, R. B.; Schaefer III, H. F.; Schleyer, P. v. R.; Robinson, G. H. *Science* **2008**, 321, 1069.
- (3) Xiong, Y.; Yao, S.; Inoue, S.; Epping, J. D.; Driess, M. *Angew. Chem. Int. Ed.* **2013**, 52, 7147; *Angew. Chem.* **2013**, 125, 7287.
- (4) Arz, M. I.; Geiß, D.; Straßmann, M.; Schnakenburg, G.; Filippou, A. C. *Chem. Sci.* **2015**, 6, 6515.
- (5) (a) Ghadwal, R. S.; Roesky, H. W.; Merkel, S.; Henn, J.; Stalke, D. *Angew. Chem. Int. Ed.* **2009**, 48, 5683; *Angew. Chem.* **2009**, 121, 5793. (b) Filippou, A. C.; Chernov, O.; Schnakenburg, G. *Angew. Chem. Int. Ed.* **2009**, 48, 5687; *Angew. Chem.* **2009**, 121, 5797. (c) Filippou, A. C.; Chernov, O.; Schnakenburg, G. *Chem. Eur. J.* **2011**, 17, 13574. (d) Filippou, A. C.; Lebedev, Y. N.; Chernov, O.; Straßmann, M.; Schnakenburg, G. *Angew. Chem. Int. Ed.* **2013**, 52, 6974; *Angew. Chem.* **2013**, 125, 7112.
- (6) (a) Filippou, A. C.; Chernov, O.; Blom, B.; Stumpf, K. W.; Schnakenburg, G. *Chem. Eur. J.* **2010**, 16, 2866. (b) Cui, H.; Cui, C. *Dalton Trans.* **2011**, 40, 11937. (c) Al-Rafia, S. M. I.; McDonald, R.; Ferguson, M. J.; Rivard, E. *Chem. Eur. J.* **2012**, 18, 13810. (d) Inoue, S.; Eisenhut, C. *J. Am. Chem. Soc.* **2013**, 135,

18315. (e) Agou, T.; Hayakawa, N.; Sasamori, T.; Matsuo, T.; Hashizume, D.; Tokitoh, N. *Chem. Eur. J.* **2014**, *20*, 9246.
- (7) Cowley, M. J.; Huch, V.; Rzepa, H. S.; Scheschkewitz, D. *Nat. Chem.* **2013**, *5*, 876.
- (8) Arz, M. I.; Straßmann, M.; Meyer, A.; Schnakenburg, G.; Schiemann, O.; Filippou, A. C. *Chem. Eur. J.* **2015**, *21*, 12509.
- (9) Ahmad, S. U.; Szilvási, T.; Inoue, S. *Chem. Commun.* **2014**, *50*, 12619.
- (10) (a) Jana, A.; Huch, V.; Scheschkewitz, D. *Angew. Chem. Int. Ed.* **2013**, *52*, 12179; *Angew. Chem.* **2013**, *125*, 12401. (b) Jana, A.; Majumdar, M.; Huch, V.; Zimmer, M.; Scheschkewitz, D. *Dalton Trans.* **2014**, *43*, 5175.
- (11) Geiß, D.; Arz, M. I.; Straßmann, M.; Schnakenburg, G.; Filippou, A. C. *Angew. Chem. Int. Ed.* **2015**, *54*, 2739; *Angew. Chem.* **2015**, *127*, 2777.
- (12) Ghana, P.; Arz, M. I.; Das, U.; Schnakenburg, G.; Filippou, A. C. *Angew. Chem. Int. Ed.* **2015**, *54*, 9980; *Angew. Chem.* **2015**, *127*, 10118.
- (13) (a) Himmel, D.; Krossing, I.; Schnepf, A. *Angew. Chem. Int. Ed.* **2014**, *53*, 370; *Angew. Chem.* **2014**, *126*, 378. (b) Frenking, G. *Angew. Chem. Int. Ed.* **2014**, *53*, 6040; *Angew. Chem.* **2014**, *126*, 6152. (c) Himmel, D.; Krossing, I.; Schnepf, A. *Angew. Chem. Int. Ed.* **2014**, *53*, 6047; *Angew. Chem.* **2014**, *126*, 6159. (d) Köppe, R.; Schnöckel, H. *Chem. Sci.* **2015**, *6*, 1199. (e) Perras, F. A.; Ewing, C. A.; Dellermann, T.; Böhne, J.; Ullrich, S.; Schäfer, T.; Braunschweig, H.; Bryce, D. L. *Chem. Sci.* **2015**, *6*, 3378.
- (14) (a) Frenking, G.; Tonner, R. In *The Chemical Bond – Chemical Bonding Across the Periodic Table*; Frenking, G., Shaik, S., Eds.; Wiley-VCH: Weinheim, 2014; chapter 4, pp. 71 – 112. (b) Holzmann, N.; Andrada, D. M.; Frenking, G. *J. Organomet. Chem.* **2015**, *792*, 139.
- (15) (a) Dyker, C. A.; Bertrand, G. *Science* **2008**, *321*, 1050. (b) Sidiropoulos, A.; Jones, C.; Stasch, A.; Klein, S.; Frenking, G. *Angew. Chem. Int. Ed.* **2009**, *48*, 9701; *Angew. Chem.* **2009**, *121*, 9881. (c) Jones, C.; Sidiropoulos, A.; Holzmann, N.; Frenking, G.; Stasch, A. *Chem. Commun.* **2012**, *48*, 9855. (d) Frenking, G.; Holzmann, N. *Science* **2012**, *336*, 1394. (e) Holzmann, N.; Dange, D.; Jones, C.; Frenking, G. *Angew. Chem. Int. Ed.* **2013**, *52*, 3004; *Angew. Chem.* **2013**, *125*, 3078.
- (16) (a) Bruna, P. J.; Peyerimhoff, S. D.; Buenker, R. J. *J. Chem. Phys.* **1980**, *72*, 5437. (b) Peyerimhoff, S. D.; Buenker, S. D. *Chem. Phys.* **1982**, *72*, 111.
- (17) The B3LYP/6-311+G**/6-31G* computed ZPVE corrected (ZPVE = zero point vibrational energy) dissociation energies for the stepwise dissociation of the carbene substituents from Si₂(Idipp)₂ at 0 K amount to 126.5 kJ mol⁻¹ (Si₂(Idipp)₂ → Si₂(Idipp) (S = 0) + Idipp (S = 0)) and 185.0 kJ mol⁻¹ (Si₂(Idipp) → Si₂ (S = 1, X³Σ_g⁻) + Idipp (S = 0)) (S is the total spin angular momentum of the electronically and geometrically relaxed fragments), see ref. [8].
- (18) For a quantum chemical description of through-bond and through-space interactions leading to n+ and n-lone pair orbitals see: (a) Hoffmann, R. *Acc. Chem. Res.* **1971**, *4*, 1. (b) Albright, T. A.; Burdett, J. K.; Whangbo, M.-H. *Orbital Interactions in Chemistry*, 2nd ed., Wiley-Interscience: Hoboken, New Jersey, 2013; chapter 11, pp. 241 – 271.
- (19) Nobel lecture on isolobal analogy: Hoffmann, R. *Angew. Chem. Int. Ed. Engl.* **1982**, *21*, 711; *Angew. Chem.* **1982**, *94*, 725.
- (20) In an approach for the formal classification of covalent compounds of transition metals, a neutral 2e-donor as Idipp has been also considered as equivalent to R⁻ (R = alkyl, aryl): Green, M. L. H. *J. Organomet. Chem.* **1995**, *500*, 127.
- (21) (a) Cowley, A. H.; Norman, N. C.; Pakulski, M. *J. Chem. Soc., Chem. Commun.* **1984**, 1054. (b) Cowley, A. H.; Kilduff, J. E.; Norman, N. C.; Pakulski, M. *J. Chem. Soc., Dalton Trans.* **1986**, 1801. (c) Partyka, D. V.;

- Washington, M. P.; Gray, T. G.; Updegraff III, J. B.; Turner II, J. F.; Protasiewicz, J. D. *J. Am. Chem. Soc.* **2009**, *131*, 10041.
- (22) (a) Chen, M.; Wang, Y.; Xie, Y.; Wei, P.; Gilliard Jr., R. J.; Schwartz, N. A.; Schaefer III, H. F.; Schleyer, P. v. R.; Robinson, G. H. *Chem. Eur. J.* **2014**, *20*, 9208. (b) Arz, M. I. Molecular Si(0) and Si(I) Compounds: Synthesis, Structure and Reactivity. Ph.D. Thesis, University of Bonn, 2015. (c) Arz, M. I.; Schnakenburg, G.; Filippou, A. C. σ and π Complexes of NHC-stabilized Disilicon(0), *Proceedings of the 14th International Symposium on Inorganic Ring Systems*, Regensburg, July 26–31, 2015. (d) Arz, M. I.; Straßmann, M.; Schnakenburg, G.; Filippou, A. C. Chemistry of NHC-stabilized Disilicon(0), *Proceedings of the 46th Silicon Symposium*, Davis, CA, June 21–24, 2015.
- (23) (a) Loss, S.; Widauer, C.; Grützmacher, H. *Angew. Chem. Int. Ed.* **1999**, *38*, 3329; *Angew. Chem.* **1999**, *111*, 3546. (b) Cowley, A. H.; Kilduff, J. E.; Norman, N. C.; Pakulski, M. *J. Am. Chem. Soc.* **1983**, *105*, 4845.
- (24) (a) Brookhart, M.; Grant, B.; Volpe Jr., A. F. *Organometallics* **1992**, *11*, 3920. (b) Taube, R.; Wache, S. *J. Organomet. Chem.* **1992**, *428*, 431.
- (25) Batsanov, S. S. *Inorg. Mat.* **2001**, *37*, 871.
- (26) φ_{NHC1} and φ_{NHC2} denotes the dihedral angle between the $\text{C}_{\text{NHC}}\text{-Si-Si-C}_{\text{NHC}}$ least-square plane and the least-square plane of the N-heterocyclic ring bonded to the Si1 and Si2 atom, respectively.
- (27) Yamaguchi, T.; Sekiguchi, A.; Driess, M. *J. Am. Chem. Soc.* **2010**, *132*, 14061.
- (28) Kinjo, R.; Ichinohe, M.; Sekiguchi, A. *J. Am. Chem. Soc.* **2007**, *129*, 26.
- (29) Chernov, O. Novel Molecular Si(II) Precursors for Synthesis of the First Compounds with Metal-Silicon Triple Bonds. Ph.D. Thesis, University of Bonn, 2012.
- (30) Agou, T.; Sugiyama, Y.; Sasamori, T.; Sakai, H.; Furukawa, Y.; Takagi, N.; Guo, J.-D.; Nagase, S.; Hashizume, D.; Tokitoh, N. *J. Am. Chem. Soc.* **2012**, *134*, 4120.
- (31) (a) Simons, R. S.; Haubrich, S. T.; Mork, B. V.; Niemeyer, M.; Power, P. P. *Main Group Chemistry* **1998**, *2*, 275. (b) Weidemann, N.; Schnakenburg, G.; Filippou, A. C. *Z. Anorg. Allg. Chem.* **2009**, *635*, 253.
- (32) Binsch, G.; Eliel, E. L.; Kessler, H. *Angew. Chem. Int. Ed. Engl.* **1971**, *10*, 570; *Angew. Chem.* **1971**, *83*, 618.
- (33) Arduengo III, A. J.; Krafczyk, R.; Schmutzler, R.; Craig, H. A.; Goerlich, J. R.; Marshall, W. J.; Unverzagt, M. *Tetrahedron* **1999**, *55*, 14523.
- (34) Iggo, J. A. *NMR Spectroscopy in Inorganic Chemistry*, Oxford University Press: Oxford, England, 1999.
- (35) Dolgonos, G. *Chem. Phys. Lett.* **2008**, *466*, 11.
- (36) Dürr, M.; Höfer, U. *Progr. Surf. Sci.* **2013**, *88*, 61.
- (37) (a) Staebler, D. L.; Wronski, C. R. *Appl. Phys. Lett.* **1977**, *31*, 292. (b) Branz, H. M. *Phys. Rev. B* **1999**, *59*, 5498.
- (38) (a) Haselbach, E.; Heilbronner, E. *Tetrahedron Lett.* **1967**, *8*, 4531. (b) Hoefnagel, M. A.; van Veen, A.; Wepster, B. M. *Rec. Trav. Chim. Pays-Bas* **1969**, *88*, 562. (c) Haselbach, E. *Helv. Chim. Acta* **1970**, *53*, 1526. (d) Eian, G. L.; Kingsbury, C. A. *Bull. Chem. Soc. Jpn.* **1970**, *43*, 739. (e) Cox, R. A.; Buncel, E. In *The chemistry of the hydrazo, azo and azoxy groups*; Patai's Chemistry of Functional Groups, Patai, S., Ed.; Wiley-Interscience: New York, 1975; Volume 2, chapter 18, pp. 775 – 859. (f) Kuroda, Y.; Lee, H.; Kuwae, A. *J. Phys. Chem.* **1980**, *84*, 3417.
- (39) For selected reviews see: (a) Leone, R. E.; Schleyer, P. v. R. *Angew. Chem. Int. Ed. Engl.* **1970**, *9*, 860; *Angew. Chem.* **1970**, *82*, 889. (b) Olah, G. A. *J. Am. Chem. Soc.* **1972**, *94*, 808. (c) Olah, G. A. *Angew. Chem. Int. Ed. Engl.* **1973**, *12*, 173; *Angew. Chem.* **1973**, *85*, 183. (d) McMurry, J. E.; Lectka, T. *Acc. Chem. Res.* **1992**, *25*, 47.

- (40) Taking the equation $\Delta G^\ddagger = 0.01914 \cdot T \cdot [9.972 + \lg(T/\Delta\nu)]$, the smallest separation ($\Delta\nu$) of two signals of the heterotopic Idipp substituents in the ^1H NMR spectrum at 298 K ($\Delta\nu = 7.6$ Hz) and the boiling point of THF- d_8 ($T = 338$ K), a low limit of the Gibbs energy of activation can be estimated to be $\Delta G^\ddagger = 75 \text{ kJ mol}^{-1}$ (Sandström, D. *Dynamic NMR Spectroscopy*; Academic Press: London, 1992).
- (41) (a) Hunter, B. K.; Reeves, L. W. *Can. J. Chem.* **1968**, *46*, 1399. (b) Schraml, J.; Chvalovský, V.; Mägi, M.; Lippmaa, E. *Coll. Czech. Chem. Commun.* **1979**, *44*, 854.
- (42) Dorman, D. E.; Jautelat, M.; Roberts, J. D. *J. Org. Chem.* **1971**, *36*, 2757.
- (43) ORCA 3.0.0 program package: (a) Neese, F. *WIREs Comput. Mol. Sci.* **2012**, *2*, 73. B97-D3 functional: (b) Grimme, S. *J. Comput. Chem.* **2006**, *27*, 1787. (c) Grimme, S.; Antony, J.; Ehrlich, S.; Krieg, H. *J. Chem. Phys.* **2010**, *132*, 154104. (d) Grimme, S.; Ehrlich, S.; Goerigk, L. *J. Comput. Chem.* **2011**, *32*, 1456. COSMO model: (e) Klamt, A.; Schüürmann, G. *J. Chem. Soc., Perkin Trans. 2* **1993**, 799. RI-JCOSX approximations: (f) Neese, F. *J. Comput. Chem.* **2003**, *24*, 1740. (g) Neese, F.; Wennmohs, F.; Hansen, A.; Becker, U. *Chem. Phys.* **2009**, *356*, 98. def2-TZVP and def2-SVP basis sets: (h) Schäfer, A.; Horn, H.; Ahlrichs, R. *J. Chem. Phys.* **1992**, *97*, 2571. (i) Weigend, F.; Ahlrichs, R. *Phys. Chem. Chem. Phys.* **2005**, *7*, 3297. NBO 6.0 program: (j) Glendening, E. D.; Badenhoop, J. K.; Reed, A. E.; Carpenter, J. E.; Bohmann, J. A.; Morales, C. M.; Landis, C. R.; Weinhold, F. Theoretical Chemistry Institute, University of Wisconsin, Madison, **2013**.
- (44) The term “ σ -bonded” isomer was used to indicate that this isomer features a Si–R σ -bond (R = H, Me, Et) resulting from the interaction of the n_+ lone pair orbital of **1** with the LUMO of the electrophile R^+ (R = H, Me, Et). In comparison, the “ π -bonded” isomer features a 3c-2e bond resulting from the interaction of the Si=Si π bond of **1** with the LUMO of the electrophile.
- (45) Holleman, A. F.; Wiberg, E. *Inorganic Chemistry*, Academic Press: San Diego/London, 2001; *Lehrbuch der Anorganischen Chemie*, 101. verbesserte und stark erweiterte Auflage, deGruyter: Berlin, 2001.
- (46) (a) Massey, A. G.; Park, A. J. *J. Organomet. Chem.* **1964**, *2*, 245. (b) Lehmann, M.; Schulz, A.; Villinger, A. *Angew. Chem. Int. Ed.* **2009**, *48*, 7444; *Angew. Chem.* **2009**, *121*, 7580.
- (47) (a) Nishida, H.; Takada, N.; Yoshimura, M.; Sonoda, T.; Kobayashi, H. *Bull. Chem. Soc. Jpn.* **1984**, *57*, 2600. (b) Bahr, S. R.; Boudjouk, P. *J. Org. Chem.* **1992**, *57*, 5545. (c) Reger, D. L.; Little, C. A.; Lamba, J. J. S.; Brown, K. J.; Krumper, J. R.; Bergman, R. G.; Irwin, M.; Fackler, J. P., Jr. *Inorg. Synth.* **2004**, *34*, 5. (d) Yakelis, N. A.; Bergman, R. G. *Organometallics* **2005**, *24*, 3579.
- (48) Scheschkewitz, D. *Angew. Chem. Int. Ed.* **2004**, *43*, 2965; *Angew. Chem.* **2004**, *116*, 3025.
- (49) Wiberg, N.; Amelunxen, K.; Lerner, H.-W.; Schuster, H.; Nöth, H.; Krossing, I.; Schmidt-Amelunxen, M.; Seifert, T. *J. Organomet. Chem.* **1997**, *542*, 1.
- (50) For a review on cation- π interactions and their importance in biological systems and material science, see: Ma, J. C.; Dougherty, D. A. *Chem. Rev.* **1997**, *97*, 1303
- (51) King, B. T.; Noll, B. C.; Michl, J. *Collect. Czech. Chem. Commun.* **1999**, *64*, 1001.
- (52) Bertermann, R.; Braunschweig, H.; Constantinidis, P.; Dellermann, T.; Dewhurst, R. D.; Ewing, W. C.; Fischer, I.; Kramer, T.; Mies, J.; Phukan, A. K.; Vargas, A. *Angew. Chem. Int. Ed.* **2015**, *54*, 13090; *Angew. Chem.* **2015**, *127*, 13282.
- (53) (a) Kira, M.; Sekiguchi, Y.; Iwamoto, T.; Kabuto, C. *J. Am. Chem. Soc.* **2004**, *126*, 12778. (b) Fischer, R.; Zirngast, M.; Flock, M.; Baumgartner, J.; Marschner, C. *J. Am. Chem. Soc.* **2005**, *127*, 70. (c) Iwamoto, T.; Sekiguchi, Y.; Yoshida, N.; Kabuto, C.; Kira, M. *Dalton Trans.* **2006**, 177. (d) Hartmann, M.; Haji-Abdi, A.; Abersfelder, K.; Haycock, P. R.; White, A. J. P.; Scheschkewitz, D. *Dalton Trans.* **2010**, 39, 9288. (e) Abe, T.; Iwamoto, T.; Kira, M. *J. Am. Chem. Soc.* **2010**, *132*, 5008.

- (54) Selected references: (a) Edlund, U.; Lejon, T.; Venkatachalam, T. K.; Buncel, E. *J. Am. Chem. Soc.* **1985**, *107*, 6408. (b) Becker, G.; Hartmann, H.-M.; Hengge, E.; Schrank, F. *Z. Anorg. Allg. Chem.* **1989**, *572*, 63. (c) Belzner, J.; Dehnert, U.; Stalke, D. *Angew. Chem. Int. Ed. Engl.* **1995**, *33*, 2450; *Angew. Chem.* **1994**, *106*, 2580. (d) Koizumi, T.; Morihashi, K.; Kikuchi, O. *Organometallics* **1995**, *14*, 4018. (e) Lee, V. Y.; Sekiguchi, A. *Organometallic Compounds of Low-Coordinate Si, Ge, Sn and Pb: From Phatom Species to Stable Compounds*, John Wiley & Sons: Chichester, West Sussex, UK, 2010; chapter 3, pp. 89 – 138. (f) Däschlein, C.; Strohmam, C. *Eur. J. Inorg. Chem.* **2009**, 43.
- (55) The ^7Li NMR resonances of π -complexed Li atoms exhibit diagnostic upfield shifts, which result from the interaction with the aromatic ring current, see: (a) Elschenbroich, C.; Salzer, A. *Organometallics. A Concise Introduction*, 2nd ed.; VCH: Weinheim, Germany, 1992. (b) Johnels, D; Günther, H In *The Chemistry of Organolithium Compounds, Part 1*; Rappoport, Z.; Marek, I., Eds.; John Wiley & Sons Ltd.: West Sussex, UK, 2004; chapter 4, pp. 137 – 204.
- (56) Mohajeri, A., Karimi, E. *J. Mol. Struct. (Theochem)* **2006**, *774*, 71.
- (57) (a) Ichinohe, M.; Sanuki, K.; Inoue, S.; Sekiguchi, A. *Organometallics* **2004**, *23*, 3088. (b) Inoue, S.; Ichinohe, M.; Sekiguchi, A. *Chem. Lett.* **2005**, *34*, 1564. (c) Iwamoto, T.; Kobayashi, M.; Uchiyama, K.; Sasaki, S.; Nagendran, S.; Isobe, H.; Kira, M.; *J. Am. Chem. Soc.* **2009**, *131*, 3156. (d) Cowley, M. J.; Abersfelder, K.; White, A. J. P.; Majumdar, M.; Scheschkewitz, D. *Chem. Commun.* **2012**, *48*, 6595. Review articles: (e) Scheschkewitz, D. *Chem. Eur. J.* **2009**, *15*, 2476. (f) Scheschkewitz, D. *Chem. Lett.* **2011**, *40*, 2.
- (58) Selected references: (a) Smit, C. N.; Lock, F. M.; Bickelhaupt, F. *Tetrahedron Lett.* **1984**, *25*, 3011. (b) Smit, C. N.; Bickelhaupt, F. *Organometallics* **1987**, *6*, 1156. (c) Bender, H. R. G.; Niecke, E.; Nieger, M. *J. Am. Chem. Soc.* **1993**, *115*, 3314. (d) Driess, M. *Coord. Chem. Rev.* **1995**, *145*, 1. (e) Driess, M., Block, S.; Brym, M.; Gamer, M. T. *Angew. Chem. Int. Ed.* **2006**, *45*, 2293; *Angew. Chem.* **2006**, *118*, 2351. (f) Yao, S.; Block, M.; Brym, M.; Driess, M. *Chem. Commun.* **2007**, 3844. (g) Lee, V. Y.; Kawai, M.; Sekiguchi, A.; Ranaivonjatovo, H.; Escudié, J. *Organometallics* **2009**, *28*, 4262. (h) Li, B.; Matsuo, T.; Hashizume, D.; Fueno, H.; Tanaka, K.; Tamao, K. *J. Am. Chem. Soc.* **2009**, *131*, 13222. (i) Hansen, K.; Szilvási, T.; Blom, B.; Inoue, S.; Epping, J.; Driess, M. *J. Am. Chem. Soc.* **2013**, *135*, 11795. (j) Willmes, P.; Cowley, M. J.; Hartmann, M.; Zimmer, M.; Huch, V.; Scheschkewitz, D. *Angew. Chem. Int. Ed.* **2014**, *53*, 2216; *Angew. Chem.* **2014**, *126*, 2248. (k) Breit, N. C.; Szilvási, T.; Inoue, S. *Chem. Eur. J.* **2014**, *20*, 9312.

TOC graphic:

